UNDERSTANDING PHASE BEHAVIOR OF POLYMER GRAFTED NANOPARTICLES

A Thesis

Presented to the Faculty of the Graduate School

of Cornell University

In Partial Fulfillment of the Requirements for the Degree of

Master of Science

by

Arjita Kulshreshtha

August 2017

ABSTRACT

Polymer grafted Nanoparticles in homopolymer solvents or PGNs have become increasingly popular in mechanical, optical and electrical applications due to their ability to improve the properties of the host matrix. Dispersion of PGNs in host matrix is necessary to achieve the desired properties in these hybrid nanomaterials. These systems transition into mixed (dispersed) and demixed (phase separated) state depending on the molecular design and interactions between the grafted polymer and host matrix, with a marked difference in properties between these two states. To establish whether a PGN system will undergo a mixed to demixed transition one needs to calculate the free energy difference between the dispersed and aggregated states.

In this work, we have utilized mesoscale modelling to calculate the free energy difference associated with the mixed to demixed transition in PGN and homopolymer system. To this end, we first use conventional Thermodynamic Integration (TI) to obtain the free energy difference along a temperature driven path. Since, a temperature driven transition path may not always be reversible, and the free energy calculation can be prone to hysteresis, we verify our results using umbrella sampling calculations, wherein we model the order parameter as a coarse-grained number density of one component in the system. We use a harmonic biasing field, based on this coarse-grained number density to

sample configurations in both the mixed and demixed regions of the phase space to obtain a free energy landscape.

To validate our method, we first obtain the free energy of mixed-demixed transition for a binary LJ fluid system at conditions where the phase behavior is already established by previous studies and we find that our predictions for the most favorable system state agree with those in literature. Next, we use this method to calculate the free energy of transition in PGN system. From the free energy landscape, we find that the energy associated with a mixed to demixed transition in this system is large, making the mixed state as the stable system state for the conditions studied. We find that our predictions, consistent with experimental observations, rule out the possibility of any stable demixed states in the systems studied.

We also study the viscoelastic behavior of PGN systems with attractive solvent and grafted chain interactions. Our preliminary results indicate that these dispersed systems show a richer viscoelastic behavior characterized by higher viscosity and storage and loss moduli on increasing loading of nanoparticles. Modifying the interaction parameters to model systems with rich physical properties ranging from waxes and gels at high loading to low viscosity fluids at low loading will provide useful insights on the viscoelastic behavior PGN systems.

BIOGRAPHICAL SKETCH

Arjita Kulshreshtha was born and brought up in Lucknow, India. After completing her schooling, she moved to Goa to pursue an undergraduate degree in Chemical Engineering from Birla Institute of Technological Sciences, Goa Campus. She joined Oracle Server Technologies as a Software Developer in 2014. Motivated by her interest in chemical engineering she moved to Cornell in August 2015 for a Master of Science Program in Chemical Engineering.

At Cornell, under the guidance of Dr. Escobedo she has been studying the phase behavior of grafted nanoparticles. Her master's thesis focuses on wetting dewetting transitions in such solvated PGN systems. After graduating from Cornell, she plans to join University of Delaware for a Doctoral Program in Chemical Engineering.

To Mummy and Papa for their unfailing love, constant motivation and endless support.

ACKNOWLEDGMENTS

I take this opportunity to express my heartfelt gratitude to my advisor Dr. Fernando Escobedo for his constant guidance and support during my Master's degree. I am indebted to his patience, motivation and encouragement. He has been an excellent mentor always finding time to listen to the petty problems and roadblocks during my research. I thank him for all the valuable things that he has taught me over this time and I consider myself fortunate to have been his student. I would also like to thank my committee member Dr. Koch for his comments and suggestions during the development of this work.

I am grateful to Escobedo group members Endian, Chris and Yangyang for interesting discussions pertaining to this research. A special mention to Sushmit and Poornima for their help during the start of my research.

Lastly, I would like to thank my significant other, Mayank for his continued love and understanding. I also thank my parents for the many years of dedication and support without which this work would not have been possible.

TABLE OF CONTENTS

CHAPTER 1

I. Introduction

Polymer Nanocomposites comprising of a polymer matrix in a Nano-filler material have become increasingly popular for mechanical[1-5], thermal[6-8], optical[9-11] and electrolytic[12-17] applications. The macroscopic properties of these materials are driven by their chemical structure and morphology. A considerable amount of work has been done in understanding the structure property relationships[21] and morphology in nanocomposites. Among these, Polymer Grafted Nanoparticles (hereafter PGN's) nanocomposites have been extensively studied because of the numerous degrees of freedom by which they can be modified to tune the composite morphology [18-23]. Some studies on PGNs in a chemically dissimilar polymer have revealed that the increased interpenetration of solvent chains into the grafting chains leads to the formation dispersed morphologies (mixed states)[24-29]. For PGNs in homopolymer matrix, it has been established how the polydispersity in grafted chains, grafting density, graft to matrix chain length ratio, nanoparticle loading, nanoparticle chemistry etc. can be used to control the dispersion state of the polymer matrix.[18,21,30-33,37-39] Recently, in addition to the dispersed and aggregated states, experiments and simulations have also confirmed the existence of anisotropic phases such as strings, sheets etc. in PGN systems. at lower grafting densities.[18,30-32,34,35] It has been theorized that these phases exist

because of competition between enthalpy gain due to particle contacts and loss of entropy of grafted chains due to the formation of these contacts.[33]

In previous studies[44], the phase behavior of PGNs with respect to the curvature of particles was mapped out, where curvature is defined as the ratio of brush height to nanoparticle size. The findings showed that some systems at higher curvatures transitioned from single-phase to two-phase states, contrasting theoretical[34] and experimental predictions where only single-phase states were reported[32]. This discrepancy was attributed to entropic effects associated with the molecular details of the systems but further studies revealed the existence of a competing dispersed phase for systems that were previously observed to be phase separated. This led to the obvious question about the stability of the observed mixed and demixed phases and the underlying phenomena that governs a mixed to demixed transition. To establish whether a PGN system will undergo a mixed-to-demixed transition, one needs to calculate the free energy difference between the dispersed and aggregated states. On the basis that such mixed-to-demixed transitions are correlated with dewetting of the corona chains, previous, simulations have suggested that dewetting occurs due to the transition of the potential of mean force (PMF) between two approaching PGNs from repulsive to attractive. [19] Recent simulations have also considered three particle interactions between an isolated PGNs and a PGN dimer to compute PMF of their interactions as a function of their relative separation and orientation[36]. To

the best of our knowledge, studies probing the mixed state and dewetting behavior of PGNs have been restricted to two or three particle systems, which do not capture all the many-body effects that may occur in bulk systems.

In this work, we attempt to calculate the Free Energy associated with mixed-to-demixed transition in PGN systems. Free Energy methods[40-43] relate the free energy of the target state to that of a reference state (of known behavior and often of known free energy), giving the difference in free energy between these two states. We use Free Energy Integration and umbrella sampling methods[40-43] to establish the difference in free energy between the mixed and demixed phases in the PGN system. First, we use conventional thermodynamic integration along a temperature path to connect the demixed and mixed states. We calculate the free energy difference by integrating the system enthalpy along this path. Second, we use umbrella sampling with a density-based biasing potential to sample, in a more reversible and controllable way, states with variable degree of mixing in the PGN based nanocomposite system. Since this latter method can be used be used to find free energy changes associated with any mixed to demixed transition, we first use it to establish the free energy change associated with such a transition in a system of binary Lennard Jones (hereafter LJ) fluid. The phase behavior of this system is well known and helped us assess the validity and effectiveness of the umbrella sampling method in predicting phase stability.

The rest of the work is organized as follows. Part 2 introduces the Model for molecular Interaction and simulation methodology. Part 3 deals with the formulation of Free Energy Methods. In Part 4, we discuss results for free energy calculation for both PGN and LJ systems. In Part 5 we close by giving concluding remarks.

II. Model for molecular interaction

2.1. PGN System

We adopt a coarse -grained model whereby the nanoparticles are modeled as spheres of radius, R_n. Each of these spheres comprises of one center particle surrounded by surface particles. The number of surface particles are chosen to tessellate the surface of the nanoparticle of radius R_n.These surface particles are modelled as purely repulsive and interact via Weeks-Chandler-Anderson (WCA) potential. An energy minimization is performed to establish their packing on to the spherical surface. Readers are referred to reference 44 for more details. Once, their packing has been determined surface beads act purely as tether points for grafted polymer chains and rigid body constraints are applied on the surface beads and center beads to ensure that they interact as a single entity. The polymer chains are tethered onto each of these surface beads making the grafting density (GD) 100% where $GD = \frac{Number\ of\ grafted\ chains}{Number\ of\ surface\ beads} \times 100$.

.

Grafted polymer chains consist of monomer beads forming linear chains of length N joined by harmonic bonds with the potential given by $U_{bond} = k\left(x_1 - x_{eq}\right)^2$ with $k = \frac{2500\epsilon}{\sigma^2}$. The system also contains free polymer chains which have the same length N as the grafted chains. The total number of these chains is chosen to be the same as the total of number of grafted chains. The non-bonded interactions are represented by the expanded Lennard-Jones (LJ) potential given by

$$U_{ij} = \begin{cases} 4\epsilon_{ij}\left[\left(\frac{\sigma_{ij}}{\left(r_{ij}-\Delta_{ij}\right)^2}\right)^{12} - \left(\frac{\sigma_{ij}}{\left(r_{ij}-\Delta_{ij}\right)^2}\right)^{6}\right] & r < r_{cut} \\ 0 & r > r_{cut} \end{cases}$$, where $r_{cut} = \Delta_{ij} + \Delta_{pair}$,

ϵ is the energy of interaction, σ is the bead diameter and Δ_{ij} is the shifting distance that ensures $U_{ij} = 0$ when particles of different sizes are in contact. Δ_{ij} is given by $\frac{D_i + \mathrm{D}_j - 1}{2}$ where D_i, D_j is the diameter of the two interacting beads. ϵ for nanoparticle-polymer, nanoparticle-nanoparticle and polymer-polymer interaction is 1.0. $r_{cut} = 2.5$ for nanoparticle – polymer and polymer-polymer, while for nanoparticle-nanoparticle it has a value of $\Delta_{pair} = 2^{\frac{1}{6}}$ which is a purely repulsive potential. The potentials are cut shifted to zero value at r_{cut}.

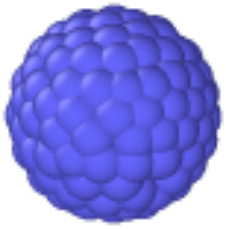

Figure 1a

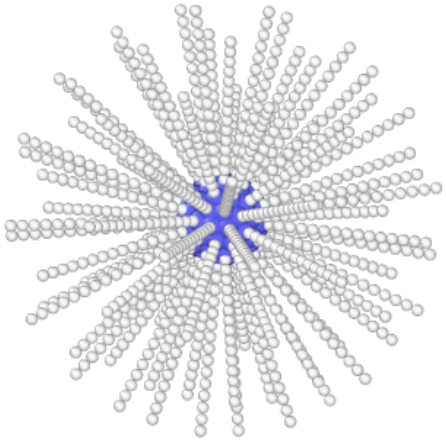

Figure 1b

Figure 1a Schematic of a bare nanoparticle of radius 3σ tessellated with 80 surface beads. Figure 1b Snapshot of a single PGN with grafted polymer beads tethered onto the nanoparticle surface. Each chain is a polymer of length 10σ.

We use LAMMPS[47] to perform MD simulations at T*= 1.0 where T* is the reduced temperature in LJ units. The radius of the nanoparticle is 3σ, the length of grafted chain and melt chain is 10σ and 80 grafted chains are tethered to each nanoparticle. The system size for conventional TI consists of 256 PGNs and for umbrella sampling calculation is reduced to 64 PGNs for computational efficiency. The equilibrated system's volume is chosen to be such that the number density (defined as ratio of the number of polymer beads to the volume not occupied by the cores) of polymer beads is 0.82 as is typical for polymer melts. We follow a rigorous equilibration protocol where initially, the PGN system is allowed to mix for 1 million timesteps at T*=3 in a large box (2~3 times

of the actual box size). After this, the box is gradually compressed over 2 million time steps to the desired box size, consistent with the density of the system. The system is then quenched from T*=3 to T*=1 in steps of $\Delta T = 0.4$ running each step for 2 million timesteps. For more simulation details the reader is referred to Reference 44. The equilibrated systems are then used as starting points for the calculation of free energy, in the NPT ensemble with a time step of 0.005 τ .

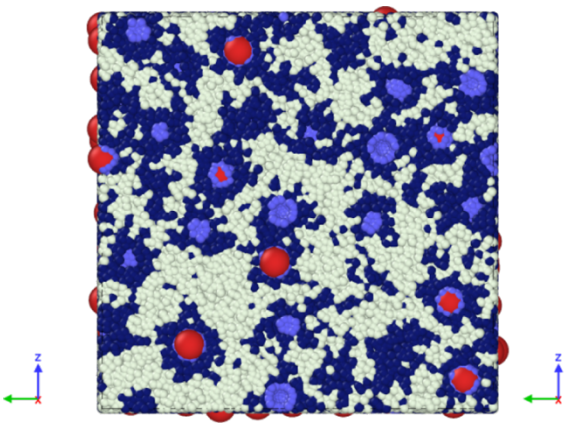

Figure 2a

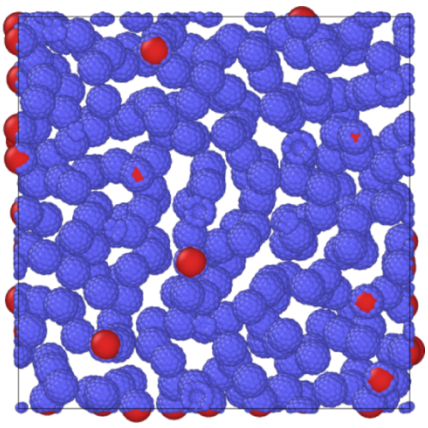

Figure 2b

Figure 2a: Coarse Grained representation of the nanoparticle melt system. The grafted chains are in shown in dark blue and free chains are shown in white. The red spheres correspond to the core beads surrounded by surface beads (in light blue). Some core beads appear bare due to the periodic boundary conditions. Figure 2b: Snapshots of bare nanoparticle cores for the system (without any grafted or free chains).

2.2. Lennard Jones Systems

The Lennard Jones fluid system consists of a binary mixture of fluids modelled as spheres of radii 0.5σ. The system consists of 500 bead of each type. These spheres interact via a LJ Potential as described in the above section. The value of ϵ is chosen to be 1 for like interactions and 0.75 for unlike interactions. This makes the interaction (contacts) between unlike particles less favorable allowing for the possibility of both mixed and demixed states in the system (depending on temperature and pressure). The potential is cut and shifted (to zero) at r_{cut}= 4σ so that no tail corrections are added.

MD Simulations are performed in LAMMPS with a time step of 0.005τ in the NPT ensemble at T*=1.15. Two values of pressure are chosen, namely P*=1.5 and P*=0.4 for system equilibration. The choice of parameters is motivated by Reference 46 in which the phase behavior of this system was mapped using the Gibbs Ensemble method and provides guidelines on the expected stable configuration of the systems.

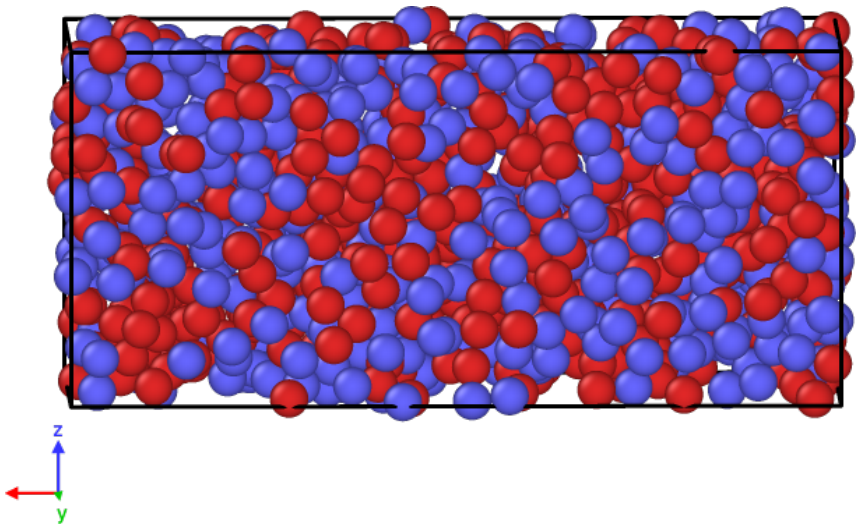

Figure 3: Coarse Grained LJ Fluid system. The system consists of 1000 beads and the two bead colors correspond to each of the two components of the binary fluid mixture. Each bead is modelled as a LJ sphere of diameter 1σ.

III. Free Energy Methods

3.1. Thermodynamic Integration in temperature.

Thermodynamic integration methods rely on sampling of a sequence of states between the target system and the reference system [42,43]. The free energy difference is evaluated via integration performed along a physical or unphysical path. In previous studies, relating PGN state to curvature, it was observed that the partially demixed PGN states transitioned into well dispersed states on increasing the temperature from T*=1 to T*=3. This can be attributed to flattening of the free energy landscape with temperature thereby reducing the barrier between mixed and demixed state and thus, temperature could be used to create a path to establish a demixed to mixed transition. The Free energy of the system can be found by integrating the system enthalpy along this path as described below

The NPT partition function for the system, $Q\ (\beta, P, N)$ is related to the Gibbs free energy of the system G by:

$$Q(\beta, P, N) = \exp(-\beta G) \qquad \text{where } \beta \text{ is } 1/kT \quad [1]$$

Letting

$$\Im = (lnQ) \qquad [2]$$

For a system at constant N, P and T,

$$d\Im = -Ud\beta - Vd(\beta P) - \beta \mathrm{u} dN \quad [3]$$

If temperature is the only variable eqn. [3] reduces to eqn. [4]

$$d\Im = -(U + PV)d\beta \quad [4]$$

$$d\Im = -Hd\beta \quad [5]$$

$$\Im = -H \int_{\beta 1}^{\beta 2} d\beta \quad [6]$$

This method can be used to calculate the difference in free energy between the states at β_1 and β_2.

Accordingly, the temperature of the systems starting at the two competing states (at low temperature), i.e., mixed and de-mixed states, is increased from T*=1 to T*=4 (i.e., β is reduced from 1 to 0.25) which allows the de mixed system to transition into a mixed state 9the only stable state at high temperature). The temperature is gradually changed in steps of $\Delta\beta = 0.075$ to minimize any hysteresis associated with a first order phase transition to the free energy calculation. The average enthalpy is numerically integrated over each $\Delta\beta$, giving the free energy as a function of β for both the systems, along the transition path. Since both systems exist in the mixed state at $\beta = 0.25$ they should have the same free energy at that point; i.e., the free energy associated with the mixed state at that temperature. Thus, any difference in free energy at $\beta = 0.25$ is

attributed to the difference in free energy between the mixed and de mixed systems at $T^* = 1$.

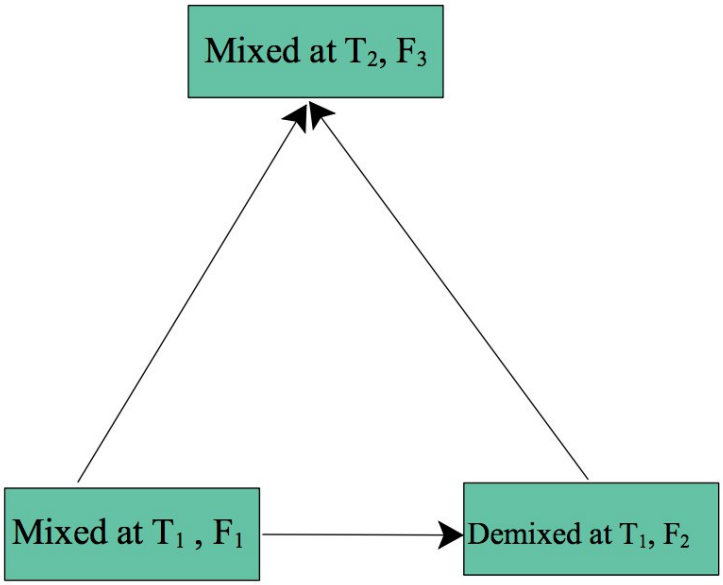

Figure 4: Illustration of the Free Energy path for Conventional TI

3.2. Umbrella Sampling

Umbrella Sampling methods are used to perform simulations along predetermined reaction coordinates[46]. They rely on utilizing a biasing potential to improve sampling along states (as defined by the reaction coordinate chosen) where the free energy barrier is large by forcing the system to achieve configurations consistent with the reaction coordinate values of interest. The appropriate biasing potential should enable a reversible transition between the states of interest over which the free energy needs to be evaluated. These states correspond to different degrees of mixing in the systems under study, and so we want to bias the system to transition from a mixed to demixed state or vice versa. For this, we use a density based ordering field to achieve a particular state of spatial mixing. The formulated ordering field is based on a harmonic potential added to the system Hamiltonian

$$U(\lambda) = \frac{1}{2}k(\lambda - \lambda_0)^2 \qquad [7]$$

which adds an energetic penalty for configurations far from λ_o. Here, k is the force constant and λ is the ordered parameter, defined as a coarse-grained number density of grafted chains occupying a region of the box extending from -R to R along the x direction as defined below.

$$\lambda = \frac{n}{N} \qquad [8]$$

where N is the total number of beads and n is the total number of grafted beads in the region of interest (-R, R), namely,

$$n = \Sigma f(x_i) \quad [9]$$

where x_i represents the i^{th} coordinate of a grafted bead and the summation extends over all beads. Since λ should be a continuous function to allow the function in Eq. (7) to be differentiable and produce a force within our molecular dynamics scheme, we define

$$f(|x_i|) = \begin{cases} 1 & p \geq 1 \\ 3p^4 - 8p^3 + 6p^2 & 0 < p < 1 \\ 0 & p \leq 0 \end{cases} \quad [10]$$

$$where\ p = \frac{R - |x_i|}{b}$$

where b is the switching distance over which the force acts. The forcing field allows for the separation between the free chains and grafted chains by controlling the number density of grafted chains inside a region of interest defined by a 1-d membrane. Thus, the field allows us to create an extended ensemble by biasing the system towards both mixed and de mixed configurations, with a target extent of mixing/demixing parametrized by the value of λ_0. The free energy is evaluated from the distribution of unbiased probabilities. Savoy et. al.[49] have previously used a variant of this method for constraining system configurations within a box for boxed molecular dynamics (BXD) simulations. The Appendix includes further details about the force implementation.

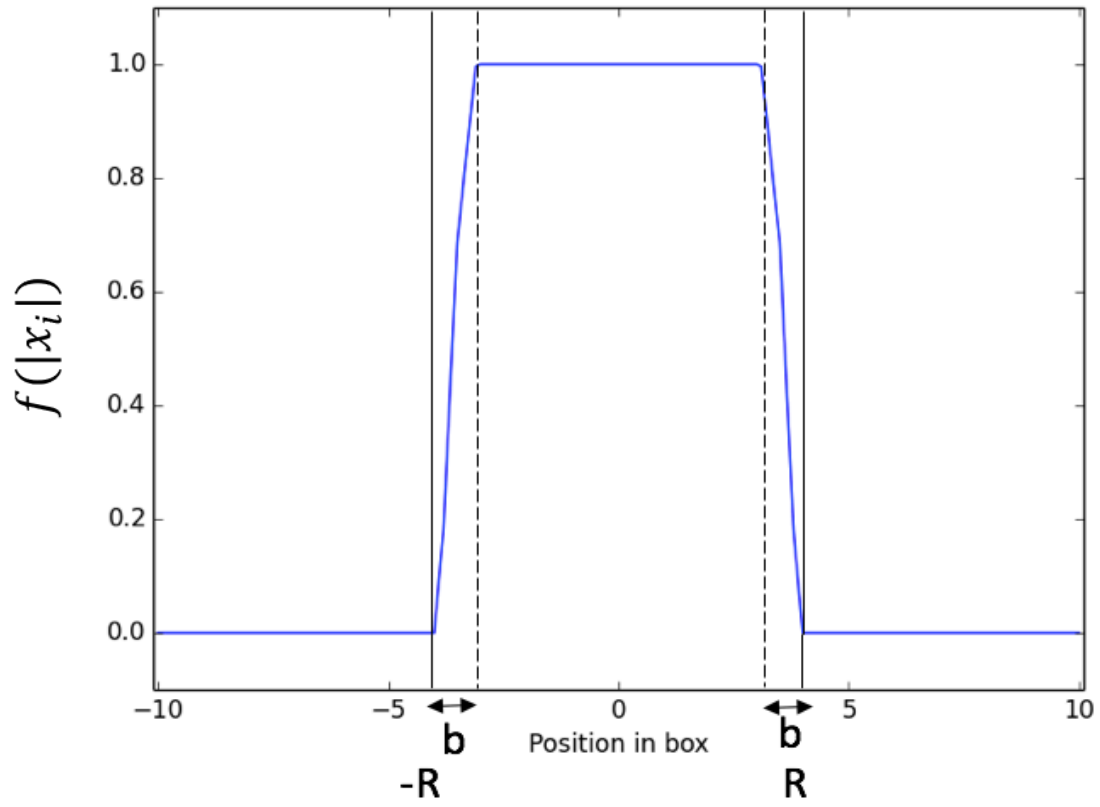

Figure 5: Representation of the coarse-grained number density of grafted beads in the system. R denotes the size of the 1-d membrane and b denotes the switching distance

For the LJ system, the forcing field controls the number density of one fluid inside the membrane by using the biasing potential to force the other fluid beads out into the bulk of the system. Table 1 summarizes the model parameters for the forcing field used for both systems

Table 1:Model Parameters for External Biasing Potential

System Type	$\boldsymbol{k}$ $[\frac{\varepsilon}{\sigma^2}]$	$\boldsymbol{R}$ [σ]	$\boldsymbol{b}$ [σ]
PGN	2.4	12	5
LJ	0.08	5.085	1

The choice of model parameters is based on the system of interest. The membrane size R is chosen based on the volume of the two phases in their respective pure states. The choice of switching distance is motivated by the relative sizes of the two components and the choice of force constant k depends on the underlying free-energy landscape of the system with respect to the order parameter. Large k values lead to a stiff forcing field which necessitates many biasing histograms to span the "λ" phase space. On the other hand, smaller k values may not be effective in biasing the configuration to the desired value of the order parameter so there exists the need to optimize the value of k for each system.

IV. Results and Discussion

4.1. Thermodynamic integration in Temperature

Figure 6a shows $\Im$ at each β value along the transition path, i.e. $\beta\ (1 \rightarrow 0.25)$. Since, β=0.25 corresponds to the mixed state for both systems, the free energy at this point should be the same. To account for this, the curve for the demixed system is shifted by the difference in free energy of the two curves at β=0.25. This adjusted curve is used in Figure 6b to show the relative Gibbs Free Energy of the system according to eqn.1 & eqn. 2

As seen from Figure 6b, the system corresponding to the mixed state has a lower free energy at β=1. It should, however be noted that this difference is small, 0.366 $k_B T$. This suggests that a mixed to de-mixed transition is not unlikely though the mixed state is more stable for $\beta > 0.62$. Also, the plot shows that, expectedly, the two Free Energy curves are comparable for all mixed states, i.e., for $\beta < 0.6$.

An underlying assumption in this calculation is that there is no hysteresis along the transition path between the mixed and de mixed states. This implies that the system should reversibly transition between both states under the influence of β. As seen from Figure 6b, the Free Energy shows a smooth transition between

the mixed and de mixed states for the PGN system (albeit this mixed-to-demixed state is not reversible due to ergodicity issues).

This method provides a preliminary estimate of the free energy changes associated with a mixing-state transition for the PGN system. The small free energy difference between the mixed and demixed states, as established by this method, motivated the development of a formal method to evaluate the free energy of transition.

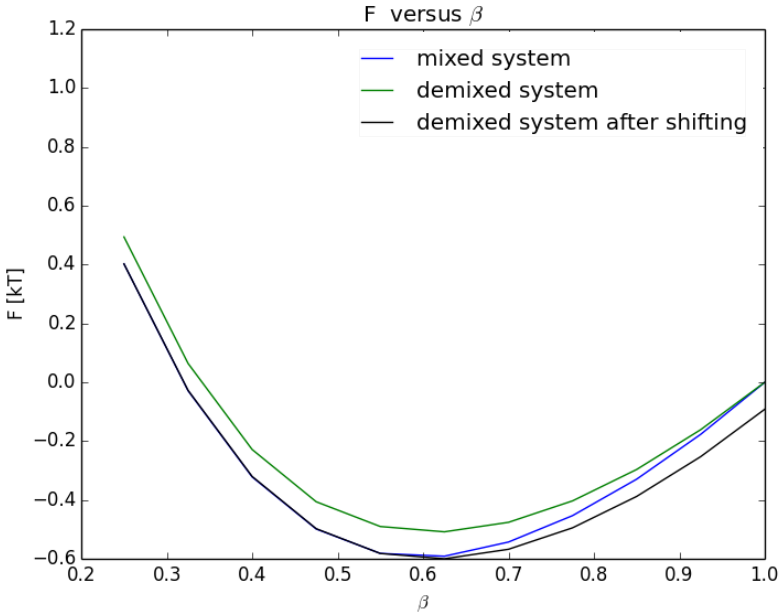

Figure 6a

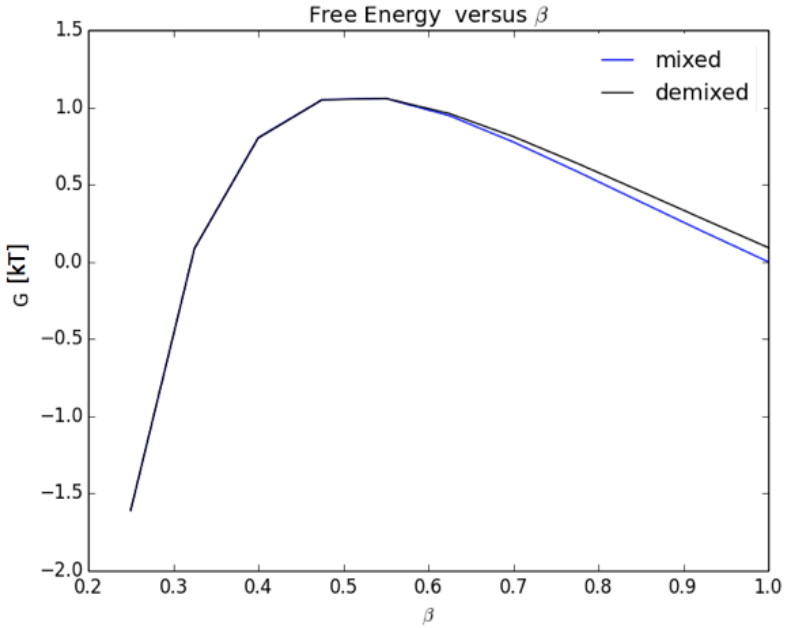

Figure 6b

Figure 6a: Plot of $\Im$ vs β for the mixed and demixed system. The curve for demixed system is shifted to obtain match the free energy in mixed state for both systems. Figure 6b: Plot of Gibbs Free Energy vs β

4.2. Umbrella Sampling with ordered parameter

4.2.1. Symmetric LJ binary Mixture

Figure 7 shows the Free Energy as a function of the order parameter λ, for a mixture of LJ Fluids at T*=1.15 and P*=1.5. Visual inspection shows that the system transitions from a mixed to a de-mixed state as λ goes from 0.26 to 0.03. The minimum of Free Energy lies at $\lambda = 0.1875$. Reference 46 described the phase diagram for this system and shows that at T*=1.15 and P*=1.5 the system consists of two phases with 0.3 and 0.7 as the mole fraction of one component in the two phases respectively. Since the order parameter, λ is a function of the coarse-grained number density of one component in the mixture, it does not directly determine the state of the system nor the relative amount of each phase if the system has two phases. We obtain concentration plots for one component of the binary LJ fluid mixture to determine the state of the system at various λ values.

Figure 8 shows the concentration profile of component 1 in the binary fluid mixture. For $\lambda = 0.26$ the amount of each component, across the box cross section, is 0.55 and 0.45 respectively, suggesting a mixed state. The system at $\lambda = 0.03$ is a two-phase mixture with 0.98 and 0.02 as mole fractions of each component in the two phases. At the minimum of Free Energy, i.e., for $\lambda = 0.1875$, the system is also a two-phase mixture where the mole fraction of one

component is 0.67 and 0.33 in the two phases. These results agree closely with Reference 46. The slight discrepancy between the amount of two phases predicted by our calculation and by the phase diagram is due to the absence of tail correction effects in our model. Indeed, previous studies have established that tail corrections can significantly alter the phase space of LJ systems[45].

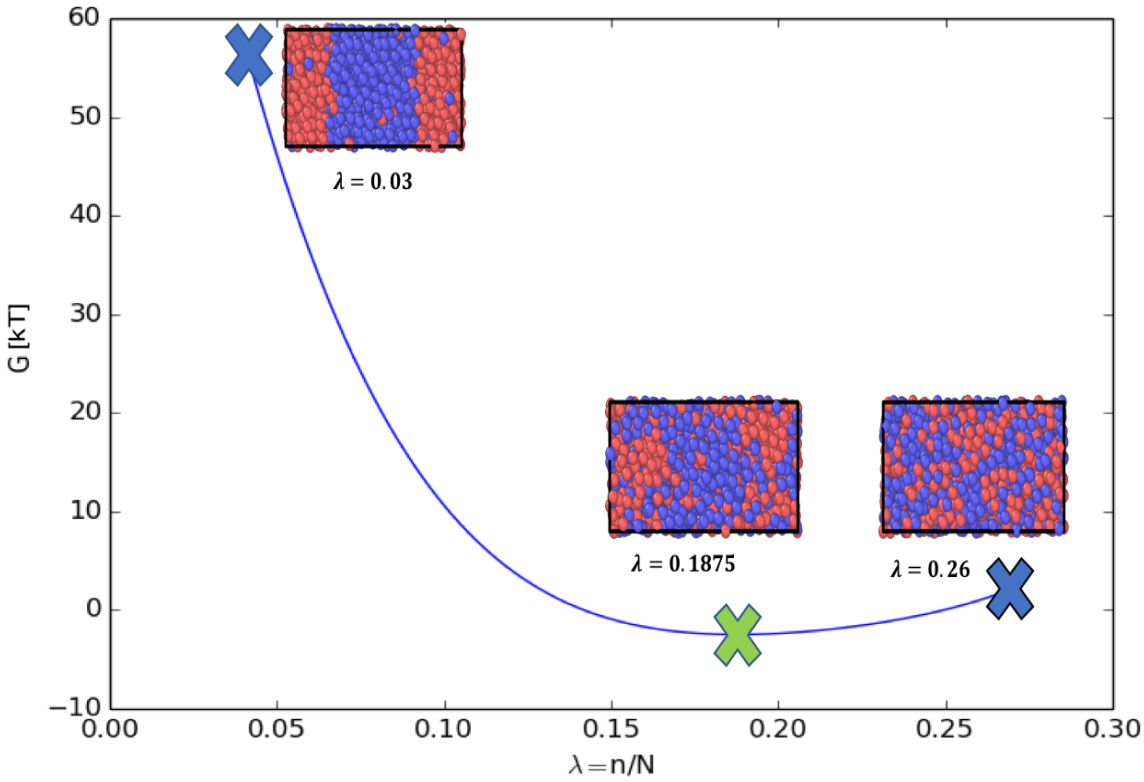

Figure 7: Plot of Gibbs Free Energy of the system w.r.t the order parameter λ for LJ fluid system at T*=1.15 and P*=1.5. Inset also shows the snapshots of the system state along the phase space.

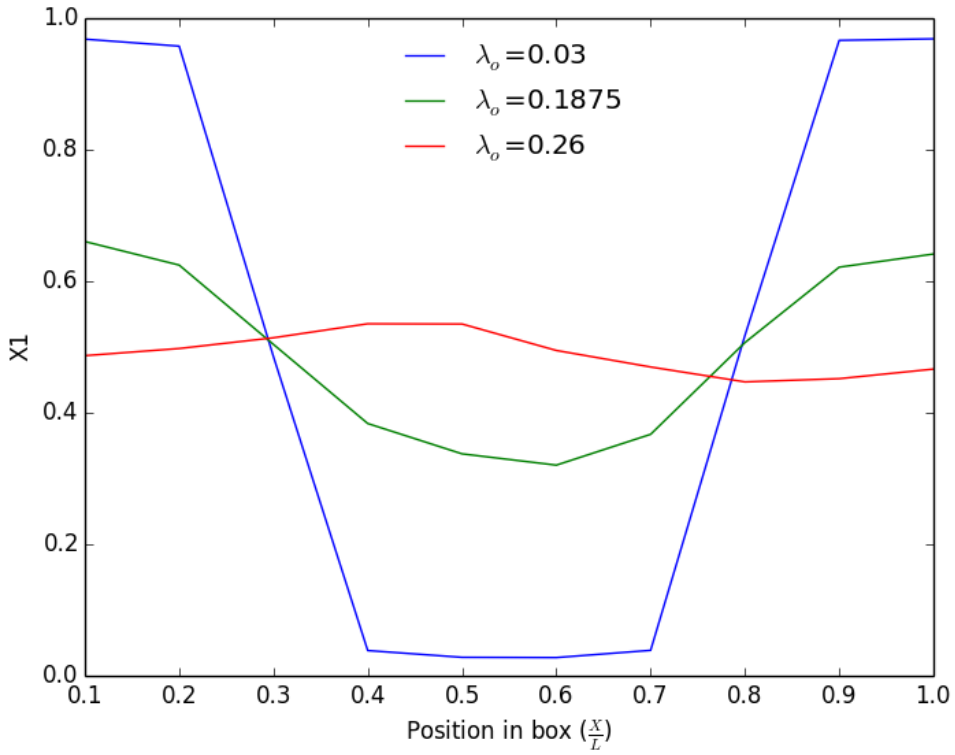

Figure 8: Concentration profile for one component of the binary LJ Fluid system at T*=1.15 and P*=1.5. The curves correspond to the system state at $\lambda = 0.26$ (red), $\lambda = 0.1875$ (green) and λ=0.03 (blue).

A similar calculation was performed for LJ fluid system at T*=1.15 and P*=0.4 where the predicted phase diagram (Reference 46) indicates a well-mixed state as stable state. Figure 9 shows the free energy as a function of λ for this system. It can be observed that the minimum of free energy lies at $\lambda = 0.212$. Concentration profiles for this system at different λ values are shown in Figure 10, which confirm that the free energy minimum corresponds to the mixed state.

This method not only predicts the stable state for an LJ system but it also establishes whether a mixed to demixed transition is feasible for the system. For the LJ system at P=1.5 the free energy minimum lies at $\lambda = 0.1875$ and is a demixed state. The free energy change between the mixed state at $\lambda = 0.26$ and the demixed state $\lambda = 0.1875$ is -4.90 $k_B T$ making this transition feasible for the system. On the other hand, for the system at P*=0.4, free energy change between a mixed state and demixed state is always positive suggesting that there are no demixed states along the phase space, while transitions toward the mixed system are always feasible.

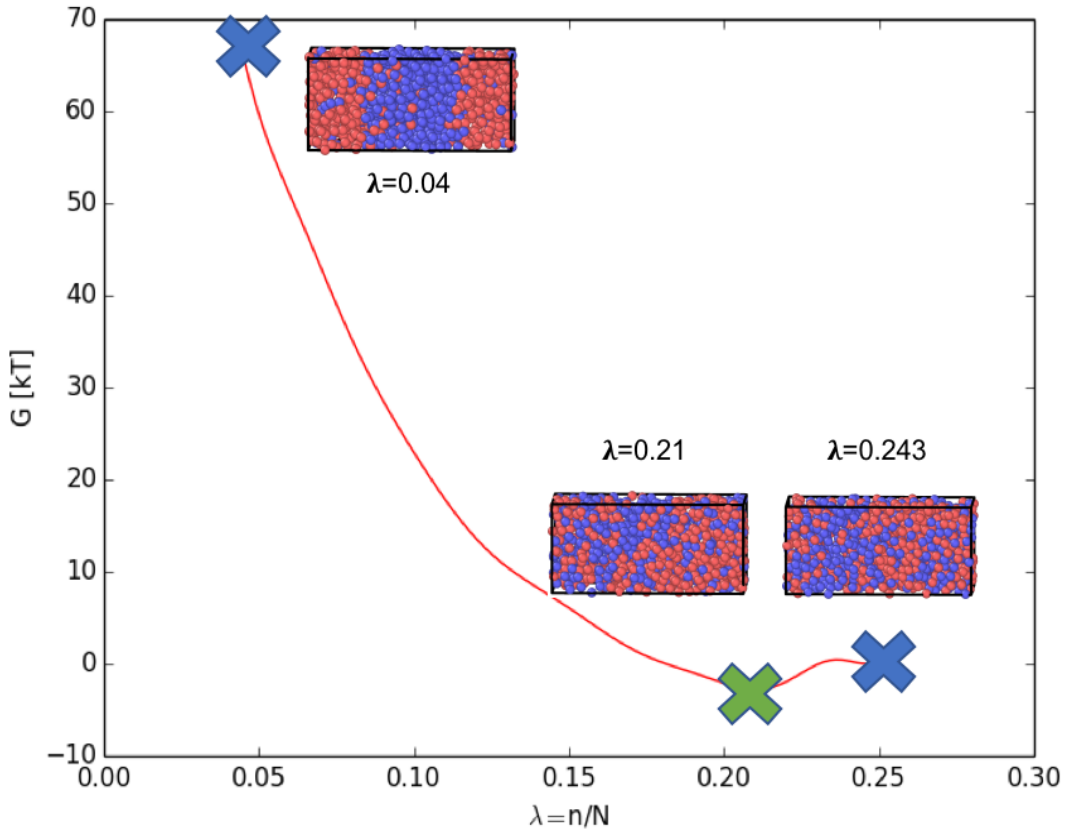

Figure 9: Plot of Gibbs Free Energy of the system w.r.t the order parameter λ for LJ fluid system at T*=1.15 and P*=0.4. Inset shows snapshots of the system state along the phase space.

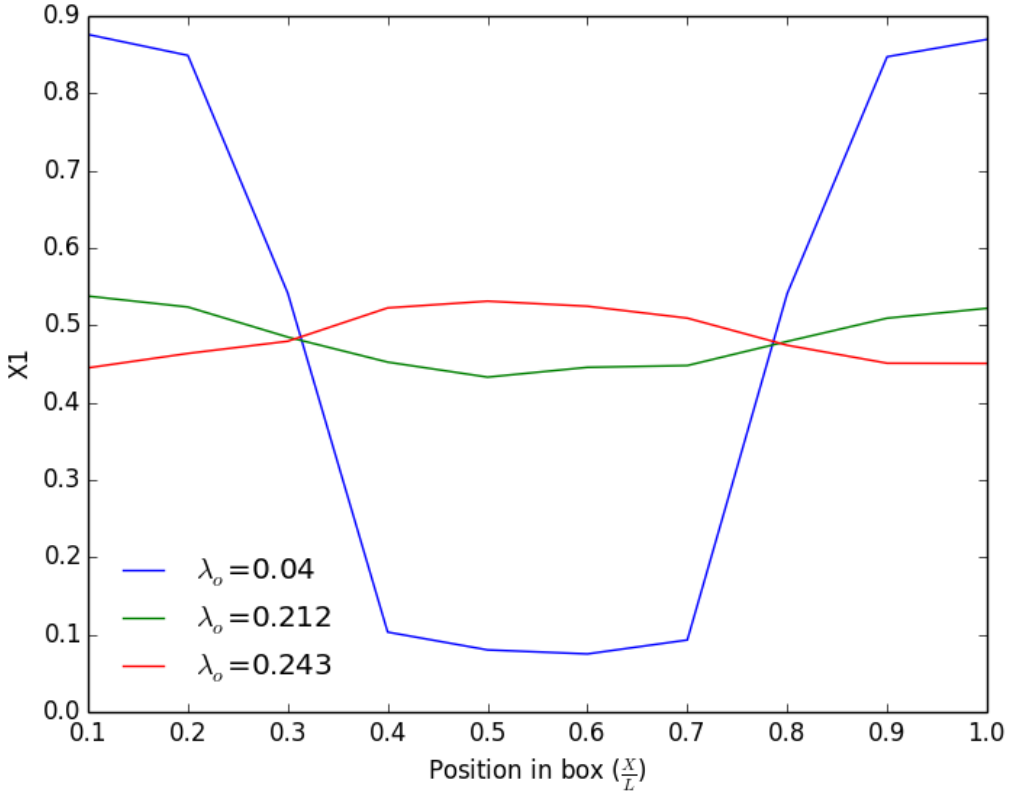

Figure 10: Concentration profile for one component of the binary LJ Fluid system at T*=1.15 and P*=0.4. The curves correspond to the system state at $\lambda = 0.243$ (red), $\lambda = 0.212$ (green) and λ=0.04 (blue).

4.2.2. PGN System

We calculate the free energy of PGN systems as a function of the order parameter λ. It is found that the system transitions from the mixed state to the demixed state as λ goes from 0.236 to 0.140. To detect the extent of phase separation in specific configurations, we construct normalized density plots[44] as shown in Figure 11.

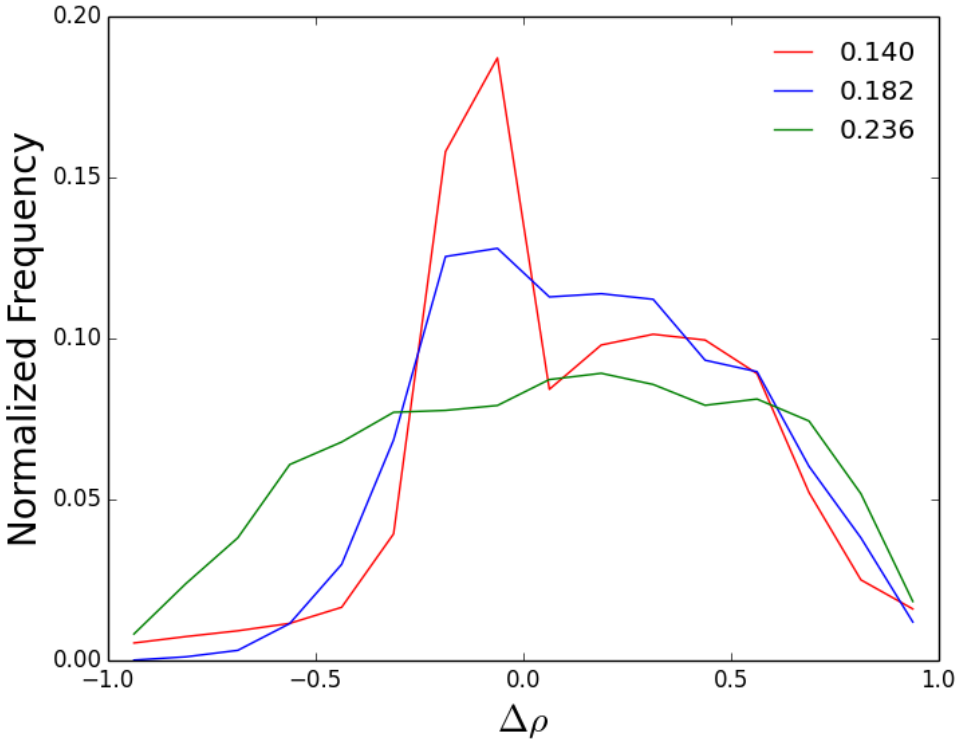

Figure 11: Normalized density plot for systems at $\lambda = 0.140$ (red), $\lambda = 0.260$ (green) and λ=0.182 (blue). Phase separation is observed as λ goes from 0.260 to 0.140 , marked by the appearance of two peaks in the distribution .For the system at $\lambda = 0.140$ (red), the two peaks corresponds to the two phases i.e. .solvent rich and corona rich ,in the system.

The density plots are constructed as follows. The system is divided into voxels of size 2 σ x2σ x 2σ. The number of grafted beads and solvent beads in each of these voxels is counted and their difference is normalized by the volume occupied by the polymer beads to get an effective density difference between grafted and solvent chains in each voxel

$$\Delta\rho = \frac{Number\ of\ grafted\ beads - Number\ of\ melt\ beads}{8\sigma^3 - Vc}$$

Vc being the core volume.

A normalized distribution for $\Delta\rho$ is plotted for the system averaged over all snapshots from the production run. Demixed systems are characterized by the presence of peaks in regions $\Delta\rho < 0$ and $\Delta\rho > 0$ corresponding to the solvent rich and nanoparticle rich regions respectively. A limitation of this method is its inability to capture phase separation associated with dewetting.

From Figure 11, it can be seen that the system transitions from mixed ($\lambda = 0.236$) to demixed ($\lambda = 0.140$) state. At $\lambda = 0.140$ each peak corresponds to the two phases (PGN rich and solvent rich) of the demixed system. The peak around $\Delta\rho \sim 0.4$ confirms the presence of a nanoparticle rich domain in the system while the peak around $\Delta\rho = -0.01$ shows the presence of a small solvent rich domain. The mixed system at $\lambda = 0.236$ is marked by a more

uniform distribution with all $\Delta\rho$ values between -0.5 and 0.5 having equal frequencies as is a characteristic of mixed systems.

We report the free energy as a function of λ in Figure 12. The free landscape resembles a cliff with mixed states lying at the minimum. The free-energy barrier height associated with a mixed to demixed is about 35kT. Another striking feature is the observance of a local minimum near the demixed state corresponding to $\lambda = 0.182$. This minimum has a well depth around the minimum of around 2kT which, being quite small, rules out the possibility of metastability in that region, contrasting results of Reference 44. It is, however, not clear how this well depth will change with system size although previous studies[48] confirm that results on the dispersion and aggregation behavior of PGNs do not change quantitatively with system size. For the system size we studied, our results indicate that mixed state is the preferred configuration for the system and a mixed to demixed transition is unlikely.

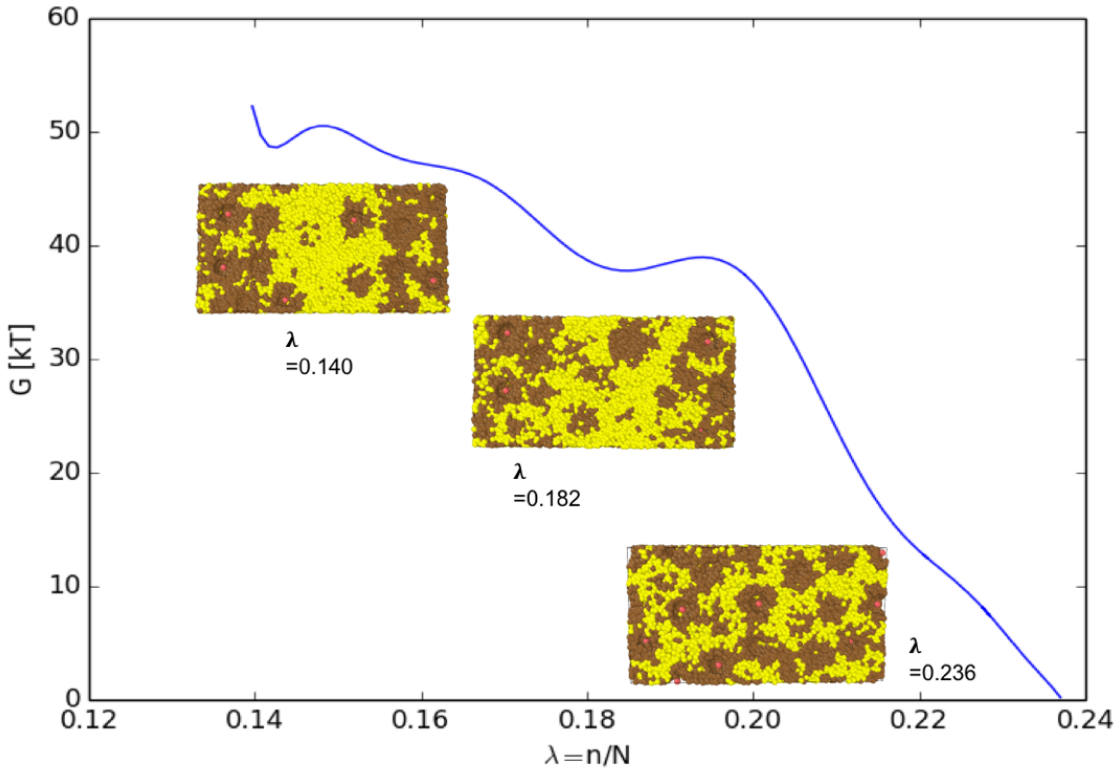

Figure 12: Plot of Gibbs Free Energy for the PGN system w.r.t the order parameter λ. Inset shows the snapshots of the system state along the phase space.

Previous studies[44], which motivated the development of this research, described the phase diagram of PGNs as a function of curvature, which is defined as ratio of radius of gyration of the grafted polymer to the nanoparticle radius. The curvature for the system studied here is about 1.05. P/N ratio, which can be defined as size of solvent to grafted chains is 1 and the systems are hence modelled to approach the high grafting density limit (100%). For such systems, previous experimental studies[21,22,35,50-52] have predicted well

dispersed PGN systems with a transition occurring only at P/N~5 and our results are hence consistent with these studies. Exceptions[53,54] to this behavior have been observed in densely grafted particles, which crystallize at high concentrations. At the conditions studied in our work, our system is not expected to crystallize nor showed any evidence of crystallization. It is also understood that conformational space and hence the entropy of a grafted chain increases with distance from the grafting surface allowing for more solvent interpenetration along the chain ends. Therefore, smaller size of the nanoparticles in comparison to grafted chains, as in the case of our system, should allow the system to have highly interpenetrated grafted chains and solvent chains (wet brush) which is a characteristic of mixed systems. These systems, should therefore favor the mixed state or exist as well dispersed systems as indicated by our results.

We believe that the anomaly in phase behavior, as observed in previous studies[44] is an artifact of the procedure used for system preparation which was seemingly incapable to allow the equilibration of grafted and melt chains. As a result, the final system state was heavily correlated to the starting configuration. After testing several equilibration protocols, we emphasize on the importance of allowing PGN systems to equilibrate at a higher temperature, at a larger box size, to facilitate mixing of grafted and solvent chains. This should be followed by compression of the box to the desired density and stepwise quenching to the

desired temperature. Similar observations have also been reported by other studies[71].

V. Conclusion

We establish the free energy difference associated with a mixed to demixed transition in a system of PGNs in a homopolymer matrix. To this end, we first use conventional Thermodynamic integration to obtain the free energy difference between mixed and demixed PGN states along a temperature driven path. Since, the possibility of hysteresis cannot be ruled out along a temperature driven transition path we use umbrella sampling to confirm our observations, whereby we model the order parameter as a coarse-grained number density of one component in the system. Our biasing field, is a harmonic function of the ordered parameter and allows us to sample configurations in both mixed and demixed regions of the phase space. As a test for our umbrella sampling method, we first obtained the free energy change for the transition between the mixed and demixed states of a binary LJ fluid mixture, a system whose phase diagram is already established. Our free energy calculations predict stable states at different conditions which agree with those reported in the literature. Next, we use this method to calculate the free energy change associated with mixing-demixing transition in a selected PGN system. From the free energy landscape, we find that free energy barrier associated with a mixed to demixed transition in this system is large (35kT), making the mixed state the stable system state for the conditions studied. We find that our predictions are

consistent with experimental observations and rule out the possibility of stable demixed state.

CHAPTER II

I. Introduction

Polymer grafted nanoparticles have attracted significant research interest due to their demonstrated ability to markedly enhance the properties of the host material. In the previous chapter, we explored how we can predict the most stable state of a configuration of a PGN nanocomposite system and found that the dispersed state is more stable for high curvature PGN systems with equal length of grafted and homopolymer matrix chains. It is also known that in a uniform dispersion, these materials are known to improve mechanical strength[1-5], hardness, thermal resistance[6-8], optical properties[9-11], conductivity[12-17,55], which makes them suitable for a wide variety of applications in the field of electronics, optics, energy storage and lubricants etc. The ability of these nanomaterials to be characterized, processed and made suitable for an application is dictated by their rheology and viscoelastic properties. Accordingly, a lot of research has been focused on the transport properties[56] and dynamics[57-62] of these materials. For this class of materials, computational studies have probed into the dynamic response of PGN and PGN's in homopolymer matrix through non-equilibrium methods to obtain viscosity and yield stress. Experimentally, it is known that addition of PGN's to a polymer matrix causes changes in the polymer and particle dynamics in the system due to confinement

and entanglement constraints and slowing down of the relaxation behavior leading to enhancement in their storage and loss modulus (as compared to the neat polymer)[64].

Recently, simulation studies[63] directed on studying the effects of nanoparticle loading and grafting densities have provided interesting insights on the viscoelastic properties of these materials suggesting that such parametric changes yield a richer viscoelastic behavior resulting in moduli enhancements (G'(ω) and G''(ω)) and slowing down of polymer relaxation. It is known[24-29] that the dispersion state of PGN'S can be controlled by using a polymer matrix with a different chemistry than the grafted chains, thereby increasing the affinity between grafts and the matrix. Experimental studies, have revealed that the of the dynamics of such unlike polymer hosts is considerably different than their counterparts with like homopolymer hosts[57,58,59] and computational studies[53] probing into the dynamics of such systems have been initiated only very recently.

In this work, we use equilibrium MD methods to study the viscoelastic behavior of PGNs in a chemically dissimilar solvent. Previously[53], studies have looked into the effect of introducing affinity between graft and matrix chains by modelling certain graft bead and matrix bead interactions to be attractive. We model such systems by introducing attractive interactions between all the graft

and matrix chains thereby ensuring that these systems exist as uniform dispersions. We try to establish the trends in stress autocorrelation, viscosity, storage and loss moduli at two different loading conditions to elucidate the role of particle loading on the properties of the dispersion.

II. Coarse grained model and simulation methodology

We use a coarse grain model for PGNs where nanoparticles are modeled as spheres of radius, R_n. The reader is referenced to Chapter 1 for more details about the model. The non-bonded interactions are represented by the expanded Lennard-Jones (LJ) potential given by

$$U_{ij} = \begin{cases} 4\epsilon_{ij}\left[\left(\frac{\sigma_{ij}}{(r_{ij}-\Delta_{ij})^2}\right)^{12} - \left(\frac{\sigma_{ij}}{(r_{ij}-\Delta_{ij})^2}\right)^{6}\right] & r < r_{cut} \\ 0 & r > r_{cut} \end{cases}, \text{ where } r_{cut} = \Delta_{ij} + \Delta_{pair},$$

ϵ is the energy of interaction, σ is the bead diameter and Δ_{ij} is the shifting distance that ensures $U_{ij} = 0$ when particles of different sizes are in contact. Δ_{ij} is given by $\frac{D_i + D_j - 1}{2}$ where D_i, D_j is the diameter of the two interacting beads. ϵ for nanoparticle-polymer, nanoparticle-nanoparticle and grafted polymer-grafted polymer interaction is 1.0, ϵ for grafted polymer and solvent polymer is made 1.2 to make the interaction between the two different chains favorable which ensures dispersion of PGNs in solvent. $\Delta_{pair} = 2.5$ For nanoparticle –

polymer and polymer-polymer, while for nanoparticle-nanoparticle it has a value of $\Delta_{pair} = 2^{\frac{1}{6}}$ which is a purely repulsive potential. The potentials are cut shifted to zero value at r_{cut}.

We create two nanoparticle systems of radius 3σ, consisting of 64 cores with grafted and melt chains as of length 10σ with 80 grafted chains tethered to nanoparticle surface. Each system corresponds to 3.85% and 5.78% loading of PGNs in the solvent which is defined by the core volume fraction in the system as $\phi_c = \frac{(number\ of\ cores)\times\frac{4\pi}{3}R_n^3}{volume\ of\ the\ box}$. The system with $\phi_c = 3.85\%$ contains 10240 melt chains while the system corresponding to $\phi_c = 5.78\%$ consists of 5120 melt chains. For comparison purposes, we also create a system of pure solvent with $\phi_c = 0\%$, consisting of 10240 polymer chains. The simulations are started in a large box which is gradually compressed to a volume V, the equilibration volume chosen to have a number density of 0.82 for the polymer beads as is typical for polymer melts. In the equilibration run, simulations are performed in the NVT ensemble at T*=1 for 1 million steps with a timestep of 0.0001τ. Production runs are performed over an additional 10 million timesteps.

III. Calculation of Viscoelastic Properties

The shear modulus $G(t)$ is computed from the stress autocorrelation function (SACF) as given in Eqn 1

$$G(t) = \frac{V}{k_B T} < \sigma_{ij}(t)\sigma_{ij}(0) > \quad (1)$$

where V is the volume of the simulation box, $< \cdots >$ denotes the ensemble average, and σ_{ij} is the ij^{th} component of the stress tensor.

For an isotropic system, the three off diagonal components of the stress tensor are equivalent and we use the average of the three stresses for the calculation of Stress Autocorrelation Function (hereafter SACF).

Shear viscosity η if calculated using the Green Kubo[66] relationship

$$\eta = \int_0^{\infty} G(t)dt \quad (2)$$

The storage modulus $G'(\omega)$ and loss modulus $G''(\omega)$ are calculated from real and complex parts of the Fourier transform of $G(t)$

$$G(\omega) = i\omega \int_0^{\infty} e^{-i\omega t}\, G(t)dt \quad (3)$$

$$G'(\omega) = \omega \int_0^{\infty} G(t)\sin(\omega t)\, dt \quad (4)$$

$$G''(\omega) = \omega \int_0^{\infty} G(t)\cos(\omega t)\, dt \quad (5)$$

To reduce the noise in data for $G(t)$ we compute running averages from 0.9t to 1.1 t for each time t based on the method described in reference 65.

IV. Results and Discussion

To establish the microstructure of PGN systems, at different loading conditions, we plot the core to core radial distribution function, shown in Figure 13. The most probable separation distance for nanoparticles, denoted by the first peak of $g(r)$ decreases for $\phi_c = 5.78\%$. This can be attributed to the fact that the system is more concentrated compared to the system at $\phi_c = 3.85\%$, which lowers the core-core separation distance. The peak height also increases slightly on loading suggesting that nanoparticle positions become more correlated. Although this is expected as increasing concentration lowers configurational entropy, we cannot generalize these results for all loading conditions. Previous studies have established that interparticle correlations increase only up to a certain critical loading fraction, owing to the anomalous hyper diffusive behavior in these materials[72]. An important point to note here is that the core- core radial distribution function for 64 nanoparticle tends to be noisy. Increasing the number of grafted particles in the system will provide better insights into the microstructure through this method.

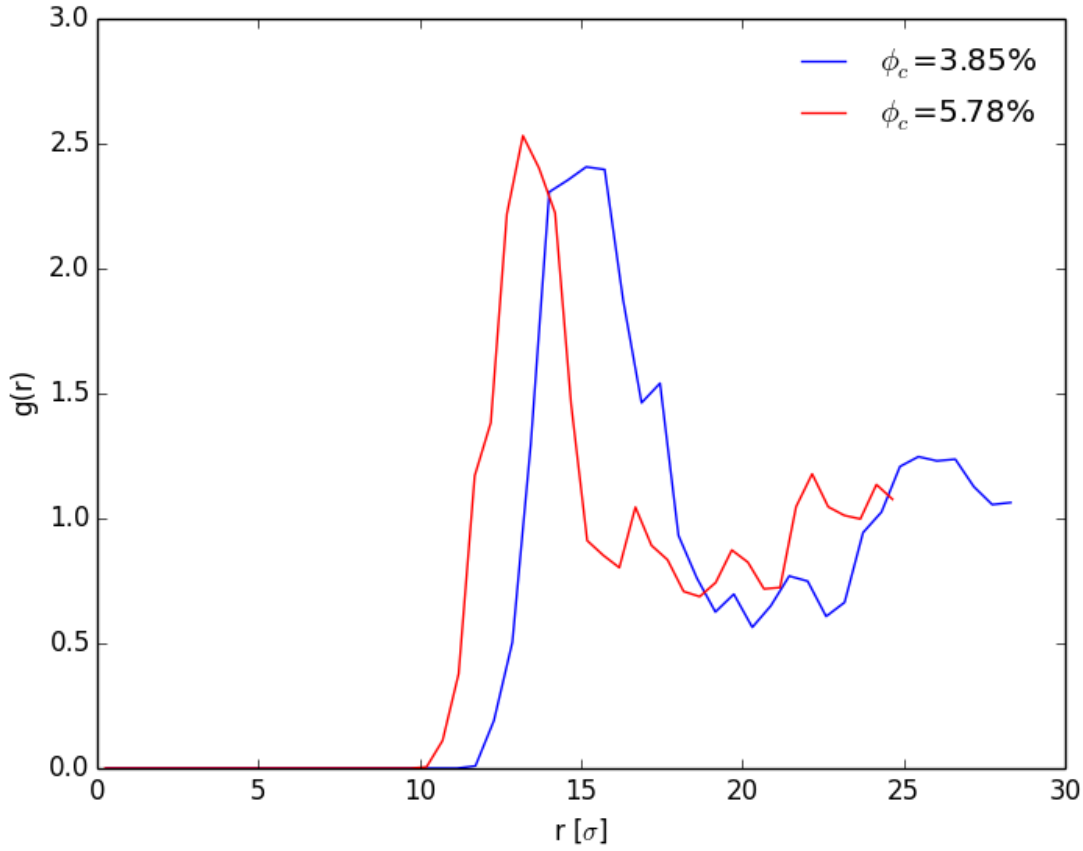

Figure 13: Core-core radial distribution function for both the nanocomposites studied here.

Figure 14 shows the short time dynamic shear modulus $G(t)$ for the two systems with loading 3.85% and 5.78% respectively. The relaxation mechanism at short times is governed by rearrangement of bonds which gives rise to fluctuations in SACF. Since this phenomenon is independent of the microstructure of the system the curves for both the systems at different loadings are comparable.

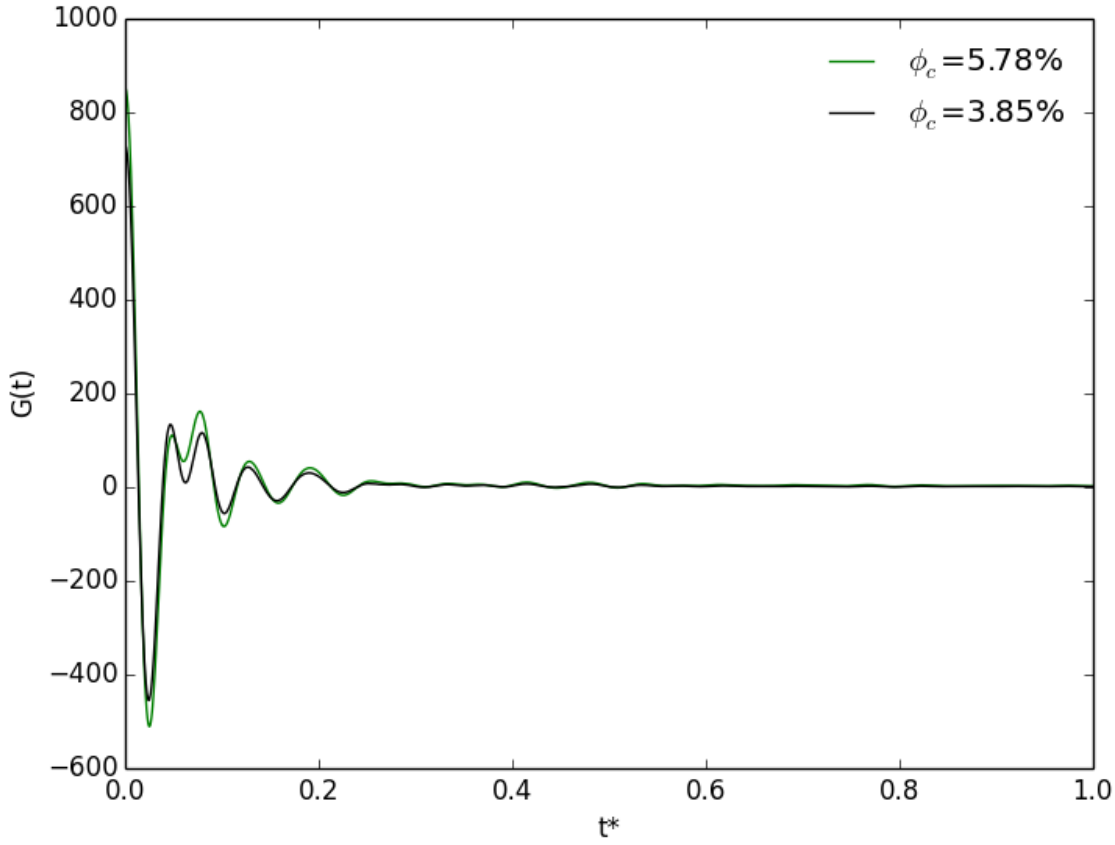

Figure 14: Short time Stress Autocorrelation function computed for both systems after averaging stresses on the off diagonal components of the system.

The SACF at intermediate time scales, as seen in Figure 15 is distinct for the two systems at different loadings. Since the grafted chains in our system have a length of N=10 and we do not expect significant entanglement effects[65,70] we adopt the Rouse Model to understand the viscoelastic behavior of the system. We find that the system at $\phi_c = 3.85\%$ follows the rouse model scaling $t^{-0.5}$at intermediate time scales. Departure from Rouse behavior is noted on increasing

the loading to $\phi_c = 5.78\%$. Our results at low loading conditions contrast the observations of a previous study[63] where introducing attractive contacts between grafted and matrix chains led to strong deviations from the Rouse behavior. The dynamics of matrix chains is strongly influenced by the interactions with their neighbors. As such, interaction with a grafted chain can slow down the relaxation of a matrix chain. For such systems, where the interactions between the grafted and melt chains are attractive, the relaxation times of matrix chains can differ depending on whether the matrix chain is bound to a free chain or a grafted chain. The heterogeneous relaxation dynamics, which becomes even more pronounced due to variable interactions brought about by introducing attractive beads along a neutral grafted chain, as in case of previous studies, can be thought to have resulted in the departure from Rouse behavior. Increase in grafted chain and matrix chain contacts and subsequent heterogeneity in matrix chain dynamics on loading causes a similar deviation for the system with $\phi_c = 5.78\%$. At longer times, we see the onset of a plateau which can be attributed to the slowing down of the relaxation of polymer chains near nanoparticles. Beyond this, $G(t)$ shows an exponential decay into the terminal regime.

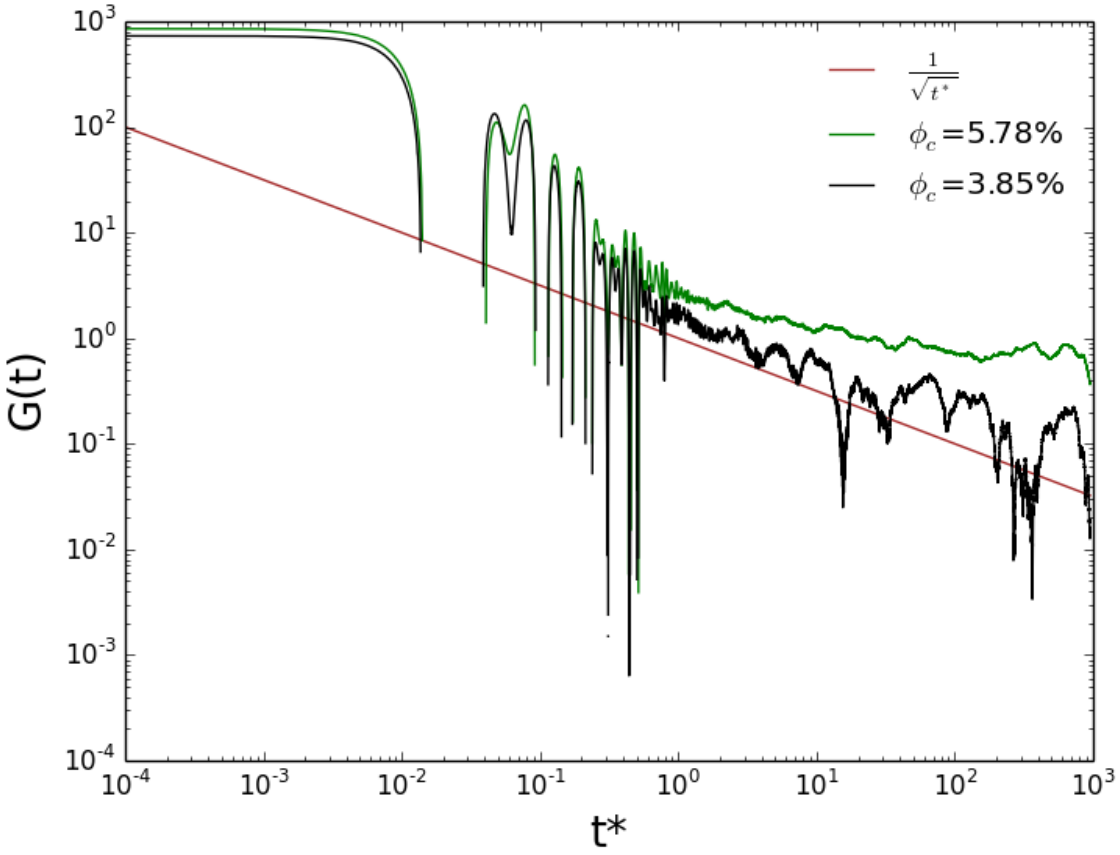

Figure 15: Stress autocorrelation function $G(t)$ vs time on a log scale. The red line denotes the expected scaling for Rouse dynamics.

We obtain the zero-shear viscosity for both systems via numerical integration of SACF over time. We observe that the reduced shear viscosity η^* increases manifold from 146 to 714 (in normalized LJ units) with increase in core volume loading from 3.85% to 5.78%. This increase in viscosity is 2 times and 11 times respectively compared to the pure solvent system. Increasing particle loading increases the caging effect in these systems reducing the translational diffusivity

of the particles and hence increasing the characteristic system relaxation times and viscosity[63]. Notably, previous studies[63] report that this enhancement in viscosity is much higher for systems with favorable corona - matrix interactions than for PGNs in homopolymer melts which suggests that tuning interactions between the grafted polymer and solvent can be effective way to enhance the viscoelastic behavior of these materials. Similar observations were also made for bare nanoparticles in polymer melts[68].

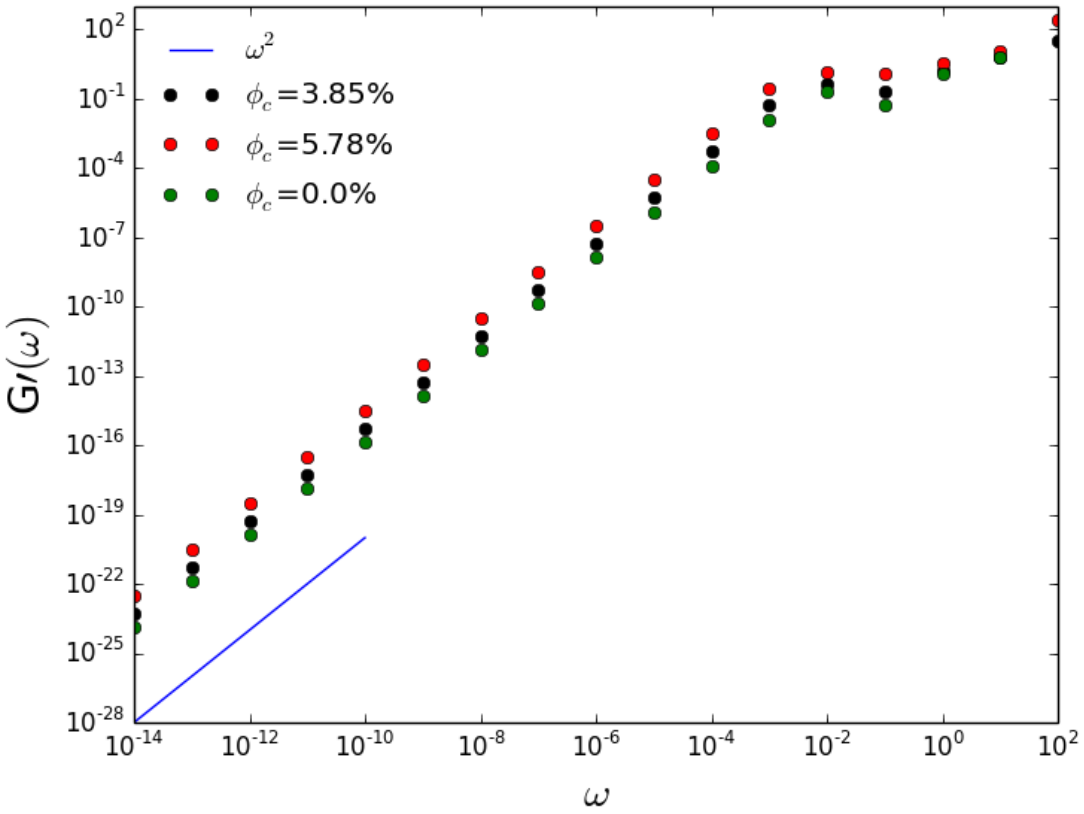

Figure 16: Storage Moduli $G'(\omega)$ for both systems. The blue line denotes a scale of ω^2 which is a characteristic for Rouse dynamics.

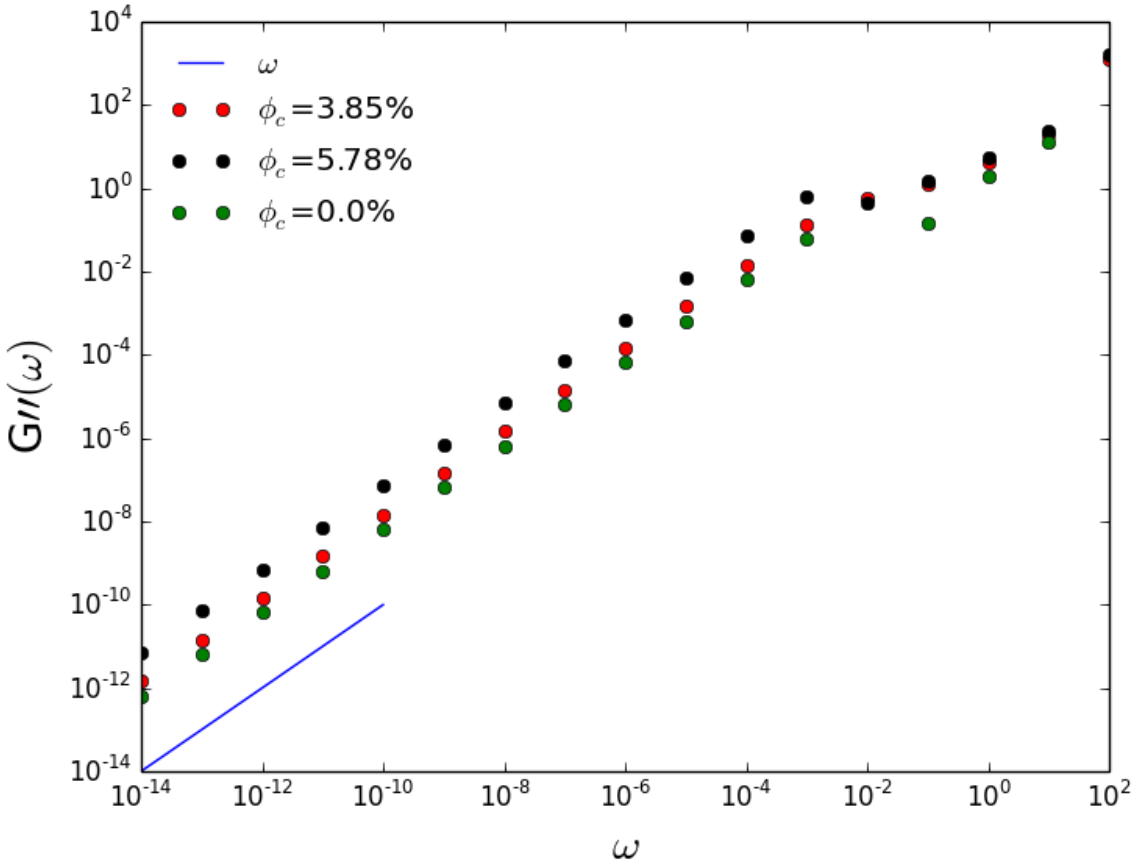

Figure 17: Loss Moduli $G''(\omega)$. The blue line denotes a scale of ω which is a characteristic for Rouse dynamics.

Next, we, compare the storage modulus $G'(\omega)$ for the two systems as shown in Figure 16. We find that the $G'(\omega)$ increases with loading, the effect being more pronounced at lower frequencies. Previous studies have reported a similar behavior, which occurs due to the increase in relaxation time of both corona and melt chains because of the additional nanoparticles. They attribute the low frequency increase in $G'(\omega)$ to the slow relaxation of chains and the high

frequency increase to the shear distortion effects due to loading[63]. At lower frequencies, it can also be seen that $G'(\omega)$ scales with ω^2 in agreement with the Rouse model indicating the presence of a terminal regime. The loss modulus $''(\omega)$, plotted in Figure 17 also shows a similar increase with particle loading, at lower frequencies. At higher frequencies, $G''(\omega)$ is comparable for the two systems. An important point here is that our coarse-grained model may not be effective in capturing the segmental dynamics governing the behavior at higher frequencies. As seen in the Figure 17, $G''(\omega)$ scales with ω, as is typical in the terminal Newtonian regime.

For the sake of comparison, we replot $G'(\omega)$ and $G''(\omega)$ together for each of the two systems. We find that at lower frequencies $G''(\omega) > G'(\omega)$ suggesting that the systems exhibit viscous behavior in this frequency range. At intermediate frequency, a crossover occurs between $G'(\omega)$ and $G''(\omega)$ and the systems, particularly the one at high loading (5.78%), show the characteristics of elastic behavior as seen by $G'(\omega) > G''(\omega)$. Both $G'(\omega)$ and $G''(\omega)$ show the evidence of a plateau at the crossover frequency. We do not expect entanglement effects is our system as our polymer chains lengths are short[70] (N=10) and we attribute this behavior to the decrease in mobility of polymer chains[63] in proximity to nanoparticles. We also note that the crossover frequency lies at $\omega^* = 0.01$, beyond which $G'(\omega)$ and $G''(\omega)$ are comparable for both systems. The dependence on $G'(\omega)$ and $G''(\omega)$ on the microstructure (in the absence of shear

distortion effects) reduces as seen by the convergence of these curves for the two systems at different loadings, in the high frequency regime.

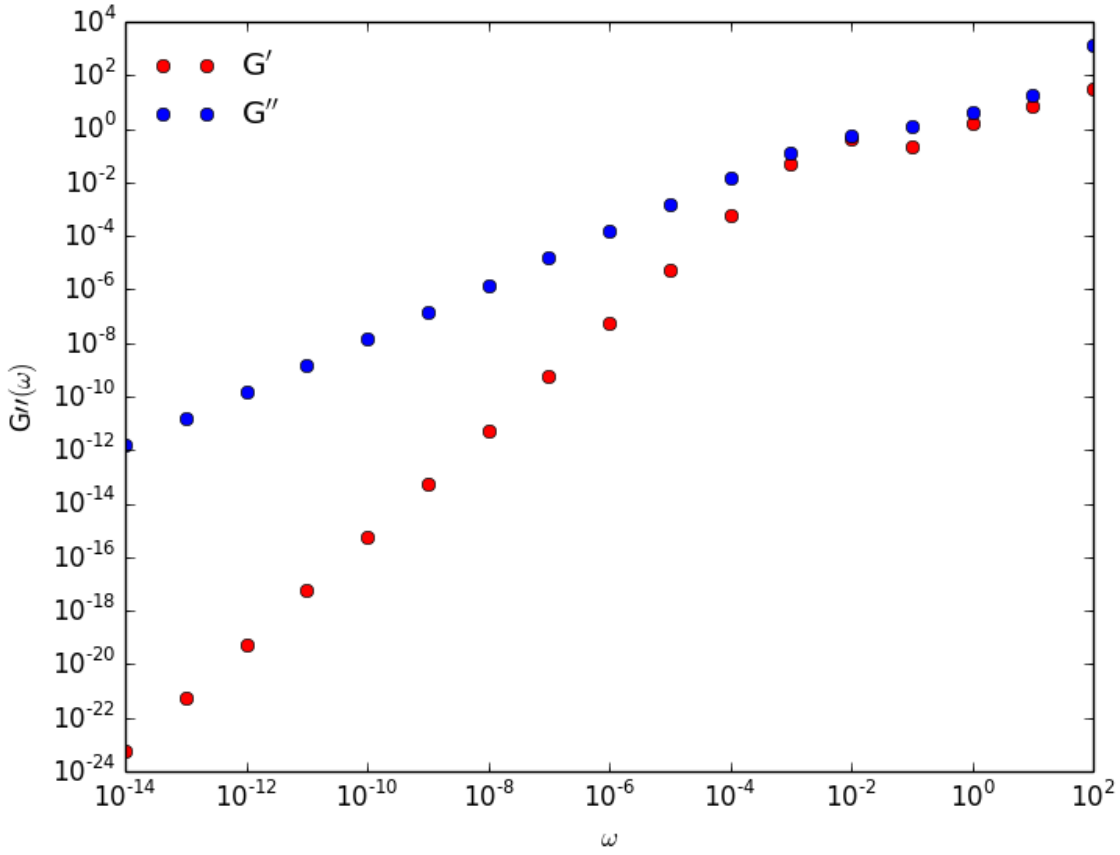

Figure 18: A comparison between the loss and storage modulus for the system with a core volume of 3.85% at a wide range of frequencies.

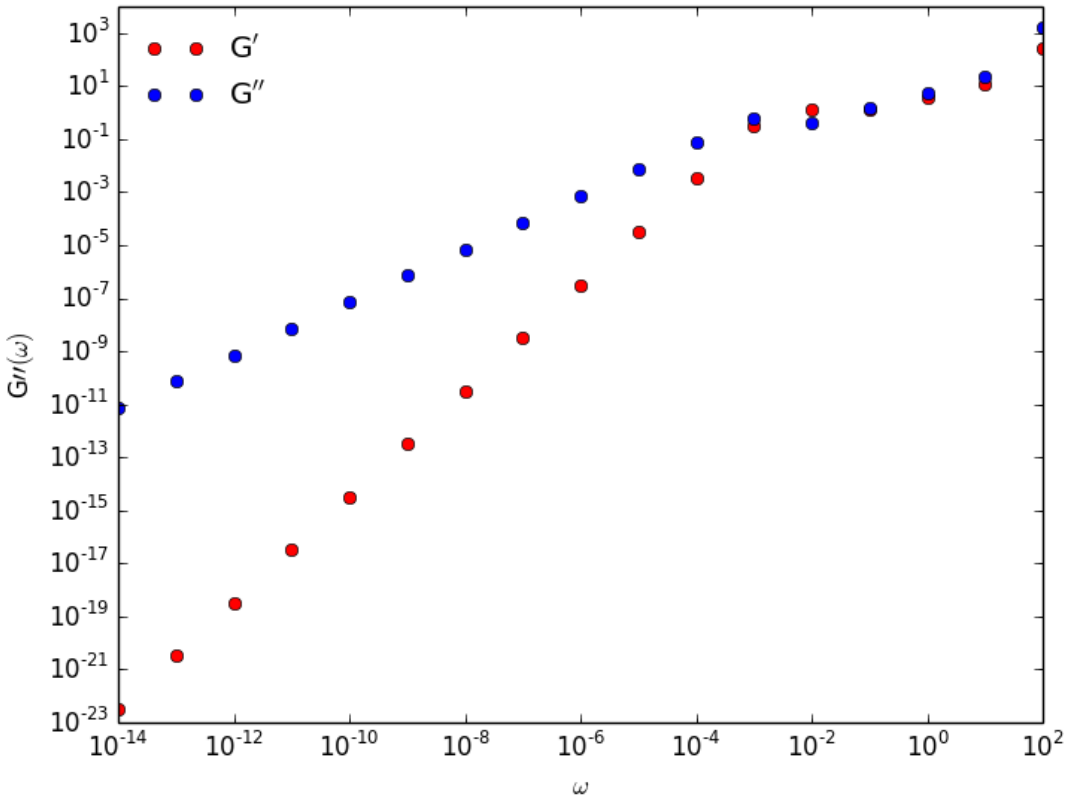

Figure 19: A comparison between the loss and storage modulus for the system with a core volume of 5.78% at a wide range of frequencies.

V. Conclusion

We conducted a preliminary study on the viscoelastic behavior of PGN based nanocomposites where the polymer matrix and grafted chains are chemically dissimilar to each other and interact via an attractive interaction potential. These nanocomposites obey Rouse Scaling exponent of $t^{-0.5}$ at shorter times and the stress autocorrelation function shows the evidence of an exponential tail. This implies that the system can be described by looking at the relaxation times of the different Rouse Modes as a measure of the system dynamics. As expected, both the loss and storage moduli also follow the expected scaling of ω and ω^2 respectively in the low frequency range. These systems show dissipative behavior at lower frequencies, marked by $G''(\omega) > G'(\omega)$ until the crossover frequency where after, both moduli have nearly the same trend and magnitude as the other. On increasing particle loading, we see an increase in both the loss and the storage modulus which can be attributed to particle induced constraints on the system. Indeed, such systems with greater affinity between grafted and free chains show signs of a richer viscoelastic behavior on increasing loading making them more suitable for industrial applications.

This study is restricted to attractive PGN nanocomposite systems that are modelled to exhibit viscous behavior over the entire frequency domain. It will be interesting to see how tuning the interaction parameter can lead to PGN

systems with χ values corresponding to those in experimental systems like PEG grafted nanoparticles in a PMMA matrix that exhibit a glassy response. For such systems, Rouse Model can be adopted to provide insights into the relaxation times of individual components i.e. the grafted and solvent chains for a different set of tuning parameters. These findings will be useful in modeling PGN systems with a targeted viscoelastic response.

APPENDIX

Quantifying LJ units

We assume that the beads are Polyethylene oxide beads, where each monomer of PEO weighs 44.05 g/mol and has a Kuhn Length of 0.77 nm. Energy scale ε is evaluated by comparing the reduced LJ temperature T*=1 to room temperature (T=273K). Thus, T*=k_bT/ε gives $\varepsilon = 3.6774 \times 10^{-21} J$ (per molecule). ($k_b = 1.380 \times 10^{-23}\, J/K$). The equilibration pressure for the systems studied is kept at P*=0.1 to keep the number density of fluid as 0.82 (defined as the number of chains beads to the volume not occupied by the cores). This gives us the measure of length scale, $\sigma = 1.54\, nm$ by comparing the pressure to atmospheric pressure. The segmental density for the beads is fixed as 0.82 $\frac{monomers}{\sigma^3}$ and on using the corresponding value of σ that we found earlier, the mass is estimated as $5.39 \times 10^{-24} kg$. We can then compute the characteristic time scale of the system, $\tau = \sigma \left(\frac{m}{\epsilon}\right)^{\frac{1}{2}}$ as 59 picoseconds making each timestep equal to 0.295 picoseconds. Based on the value of mass and chain length, we can estimate the molecular weight of the chains to be 32.5 kg/mol.

Biasing Force Field

The biasing potential is given by the following equation

$$U(\lambda) = \frac{1}{2}k(\lambda - \lambda_0)^2$$

The biasing force $F(\lambda)$ acting on grafted beads due to the above potential is defined as

$F(\lambda) = \frac{d(U(\lambda))}{dx} = -sgn * \frac{k}{N}(\ n - \ n_0)\frac{dn}{dx}$, sgn =1 if $x_i > 0$ and -1 otherwise and x_i is the coordinate of an i^{th} grafted bead. This leads to the following definition of the force acting on particles

$$\frac{df}{dx} = \begin{cases} 0, \ p < 0 \ or \ p > 1 \\ \frac{-12p(1-p)^2}{b} \ \ 0 < p < 1 \end{cases}$$

$$where \ p = \frac{R - |x_i|}{b}$$

We use a custom Fix with the above force definition to implement the biasing potential in LAMMPS.

Umbrella Sampling: Obtaining Unbiased Probabilities from Biased Histograms

Umbrella sampling methods involve calculation of free energy along a reaction coordinate from probability distributions obtain from biased histograms along that coordinate. These probabilities need to be unweighted to remove the effect external biasing potential on the probability distribution. In the NPT ensemble, this can be done in the following manner.

From statistical thermodynamics, we know,

$(U(\lambda) + PV(\lambda))^w$=$(U(\lambda) + PV(\lambda))^u$+ $\frac{k}{2}(\lambda - \lambda_o)^2$, where w & u refer to weighted and unweighted Hamiltonians of the system respectively and the harmonic term refers to the external biasing potential. Since microstate probability is defined as $e^{\Sigma(U+PV)}$ in the NPT ensemble, unweighted probability can be obtained from weighted distributions in the following manner $P^u(\lambda)$=$P^w(\lambda)e^{-\beta}\frac{k}{2}(\lambda - \lambda_o)^2$

REFERENCES

1. Tjong, Sie Chin. "Structural and mechanical properties of polymer nanocomposites." Materials Science and Engineering: R: Reports 53.3 (2006): 73-197.
2. Crosby, Alfred J., and Jong-Young Lee. "Polymer nanocomposites: the “nano” effect on mechanical properties." Polymer reviews 47.2 (2007): 217-229.
3. Akcora, Pinar, et al. ""“Gel-like” mechanical reinforcement in polymer nanocomposite melts." Macromolecules 43.2 (2009): 1003-1010.
4. Fang, Ming, et al. "Covalent polymer functionalization of graphene nanosheets and mechanical properties of composites." Journal of Materials Chemistry 19.38 (2009): 7098-7105.
5. Lin, Ning, et al. "Effects of polymer-grafted natural nanocrystals on the structure and mechanical properties of poly (lactic acid): A case of cellulose whisker-graft-polycaprolactone." Journal of Applied Polymer Science 113.5 (2009): 3417-3425.
6. Han, Zhidong, and Alberto Fina. "Thermal conductivity of carbon nanotubes and their polymer nanocomposites: a review." Progress in polymer science36.7 (2011): 914-944.
7. Leszczyńska, A., et al. "Polymer/montmorillonite nanocomposites with improved thermal properties: Part I. Factors influencing thermal stability and

mechanisms of thermal stability improvement." Thermochimica Acta 453.2 (2007): 75-96.

8. Marconnet, Amy M., et al. "Thermal conduction in aligned carbon nanotube–polymer nanocomposites with high packing density." ACS nano 5.6 (2011): 4818-4825.
9. Yano, Kazuhisa, Arimitsu Usuki, and Akane Okada. "Synthesis and properties of polyimide-clay hybrid films." Journal of Polymer Science Part A: Polymer Chemistry 35.11 (1997): 2289-2294.
10. Tamborra, M., et al. "Optical properties of hybrid composites based on highly luminescent CdS nanocrystals in polymer." Nanotechnology 15.4 (2004): S240.
11. Krebs, Frederik C., and Holger Spanggaard. "Significant improvement of polymer solar cell stability." Chemistry of materials 17.21 (2005): 5235-5237.
12. Chen, Hsien-Wei, Tzu-Pin Lin, and Feng-Chih Chang. "Ionic conductivity enhancement of the plasticized PMMA/LiClO 4 polymer nanocomposite electrolyte containing clay." Polymer 43.19 (2002): 5281-5288.
13. Croce, F., et al. "Nanocomposite polymer electrolytes for lithium batteries." Nature 394.6692 (1998): 456.

14. Vaia, Richard A., et al. "New polymer electrolyte nanocomposites: Melt intercalation of poly (ethylene oxide) in mica-type silicates." Advanced Materials 7.2 (1995): 154-156.
15. Nugent, Jennifer L., Surya S. Moganty, and Lynden A. Archer. "Nanoscale organic hybrid electrolytes." Advanced Materials 22.33 (2010): 3677-3680.
16. Choudhury, Snehashis, et al. "A highly reversible room-temperature lithium metal battery based on crosslinked hairy nanoparticles." Nature communications 6 (2015): 10101.
17. Krawiec, W., et al. "Polymer nanocomposites: a new strategy for synthesizing solid electrolytes for rechargeable lithium batteries." Journal of Power Sources 54.2 (1995): 310-315.
18. Akcora, Pinar, et al. "Anisotropic self-assembly of spherical polymer-grafted nanoparticles." Nature materials 8.4 (2009): 354.
19. Meng, Dong, et al. "Effective interactions between grafted nanoparticles in a polymer matrix." Soft Matter 8.18 (2012): 5002-5010.
20. Srivastava, S., et al. "Communication: Unusual dynamics of hybrid nanoparticles and their binary mixtures." (2010): 151105.
21. Kumar, Sanat K., et al. "Nanocomposites with polymer grafted nanoparticles." Macromolecules 46.9 (2013): 3199-3214.
22. Green, Peter F. "The structure of chain end-grafted nanoparticle/homopolymer nanocomposites." Soft Matter 7.18 (2011): 7914-7926.

23. Srivastava, Samanvaya, Jung Hwan Shin, and Lynden A. Archer. "Structure and rheology of nanoparticle–polymer suspensions." Soft Matter 8.15 (2012): 4097-4108.
24. Martin, Tyler B., et al. "Wetting–dewetting and dispersion–aggregation transitions are distinct for polymer grafted nanoparticles in chemically dissimilar polymer matrix." Journal of the American Chemical Society 137.33 (2015): 10624-10631.
25. Borukhov, Itamar, and Ludwik Leibler. "Enthalpic stabilization of brush-coated particles in a polymer melt." Macromolecules 35.13 (2002): 5171-5182.
26. Borukhov, Itamar, and Ludwik Leibler. "Stabilizing grafted colloids in a polymer melt: Favorable enthalpic interactions." Physical Review E 62.1 (2000): R41.
27. Laub, Charles F., and Jeffery T. Koberstein. "Effect of Brush Polydispersity on the Interphase between End-Grafted Brushes and Polymeric Matrixes." Macromolecules 27.18 (1994): 5016-5023.
28. Müller, M., et al. "Nano-dewetting: Interplay between van der Waals-and short-ranged interactions." The Journal of Chemical Physics 115.21 (2001): 9960-9969.
29. Kim, Bokyung, et al. "Dewetting of PMMA on PS– brush substrates." Macromolecules 42.20 (2009): 7919-7923.

30. Bedrov, Dmitry, Grant D. Smith, and Liwei Li. "Molecular dynamics simulation study of the role of evenly spaced poly (ethylene oxide) tethers on the aggregation of C60 fullerenes in water." Langmuir 21.12 (2005): 5251-5255.
31. Jiao, Yang, and Pinar Akcora. "Assembly of polymer-grafted magnetic nanoparticles in polymer melts." Macromolecules 45.8 (2012): 3463-3470.
32. Koerner, Hilmar, et al. "Nonisotropic self-organization of single-component hairy nanoparticle assemblies." ACS Macro Letters 2.8 (2013): 670-676.
33. Pryamtisyn, Victor, et al. "Modeling the anisotropic self-assembly of spherical polymer-grafted nanoparticles." (2009): 221102.
34. Xu, Chen, et al. "Dispersion of polymer-grafted magnetic nanoparticles in homopolymers and block copolymers." Polymer 49.16 (2008): 3568-3577.
35. Srivastava, Samanvaya, Praveen Agarwal, and Lynden A. Archer. "Tethered nanoparticle–polymer composites: phase stability and curvature." Langmuir28.15 (2012): 6276-6281.
36. Tang, Tsung-Yeh, and Gaurav Arya. "Anisotropic Three-Particle Interactions between Spherical Polymer-Grafted Nanoparticles in a Polymer Matrix." Macromolecules 50.3 (2017): 1167-1183.
37. Chevigny, Chloé, et al. "Polymer-grafted-nanoparticles nanocomposites: dispersion, grafted chain conformation, and rheological behavior." Macromolecules 44.1 (2010): 122-133.

38. Klos, Jaroslaw., and Tadeusz Pakula. "Interaction of a spherical particle with linear chains. II. Chains end-grafted at the particle surface." The Journal of Chemical Physics 118.16 (2003): 7682-7689.
39. Klos, Jaroslaw, and Tadeusz Pakula. "Computer simulations of chains end-grafted onto a spherical surface. Effect of matrix polymer." Macromolecules37.21 (2004): 8145-8151.
40. Kumar, Shankar, et al. "The weighted histogram analysis method for free-energy calculations on biomolecules. I. The method." Journal of computational chemistry 13.8 (1992): 1011-1021.
41. Jarzynski, Christopher. "Nonequilibrium equality for free energy differences." Physical Review Letters 78.14 (1997): 2690.
42. McQuarrie, Donald Allan. "Statistical thermodynamics." (1973).
43. Frenkel, Daan, and Berend Smit. Understanding molecular simulation: from algorithms to applications. Vol. 1. Academic press, 2001.
44. Goyal, Sushmit Sunil Kumar. "Understanding the Macroscopic Properties of Polymer Grafted Nanoparticles by Meso-Scale Modeling."
45. Smit, B. "Phase diagrams of Lennard-Jones fluids." The Journal of chemical physics 96.11 (1992): 8639-8640.
46. Georgoulaki, Aikaterini M., Dimitrios P. Tassios, and Athanassios Z. Panagiotopoulos. "Phase equilibria of binary Lennard-Jones mixtures: simulation and van der Waals I-fluid theory." Fluid Phase Equilibria 100 (1994): 153-170.

47. S. Plimpton. “Fast Parallel Algorithms for Short-Range Molecular Dynamics”. J Comp Phys 117 (1995): 1-19

48. Martin, Tyler B., and Arthi Jayaraman. "Using Theory and Simulations To Calculate Effective Interactions in Polymer Nanocomposites with Polymer-Grafted Nanoparticles." Macromolecules 49.24 (2016): 9684-9692.

49. Savoy, Elizabeth S., and Fernando A. Escobedo. "Simulation study of free-energy barriers in the wetting transition of an oily fluid on a rough surface with reentrant geometry." Langmuir 28.46 (2012): 16080-16090.

50. Kim, Daniel, et al. "Polymer nanocomposites: polymer and particle dynamics." Soft Matter 8.42 (2012): 10813-10818

51. Chevigny, Chloé, et al. "Polymer-grafted-nanoparticles nanocomposites: dispersion, grafted chain conformation, and rheological behavior." Macromolecules 44.1 (2010): 122-133.

52. Sunday, Daniel, Jan Ilavsky, and David L. Green. "A phase diagram for polymer-grafted nanoparticles in homopolymer matrices." Macromolecules45.9 (2012): 4007-4011.

53. Ohno, Kohji, et al. "Suspensions of silica particles grafted with concentrated polymer brush: Effects of graft chain length on brush layer thickness and colloidal crystallization." Macromolecules 40.25 (2007): 9143-9150.

54. Goel, Vivek, et al. "Structure of polymer tethered highly grafted nanoparticles." Macromolecules 44.20 (2011): 8129-8135.
55. Tanaka, Toshikatsu, G. C. Montanari, and R. Mulhaupt. "Polymer nanocomposites as dielectrics and electrical insulation-perspectives for processing technologies, material characterization and future applications." IEEE transactions on Dielectrics and Electrical Insulation 11.5 (2004): 763-784.
56. Goyal, Sushmit, and Fernando A. Escobedo. "Structure and transport properties of polymer grafted nanoparticles." The Journal of chemical physics135.18 (2011): 184902.
57. Mangal, Rahul, Samanvaya Srivastava, and Lynden A. Archer. "Phase stability and dynamics of entangled polymer-nanoparticle composites." Nature communications 6 (2015).
58. Mangal, Rahul, et al. "Size-dependent particle dynamics in entangled polymer nanocomposites." Langmuir 32.2 (2016): 596-603.
59. Kim, Sung A., Rahul Mangal, and Lynden A. Archer. "Relaxation dynamics of nanoparticle-tethered polymer chains." Macromolecules 48.17 (2015): 6280-6293.
60. Krishnamoorti, Ramanan, Richard A. Vaia, and Emmanuel P. Giannelis. "Structure and dynamics of polymer-layered silicate nanocomposites." Chemistry of Materials 8.8 (1996): 1728-1734.

61. Schneider, G. J., et al. "Dynamics of entangled chains in polymer nanocomposites." Macromolecules 44.15 (2011): 5857-5860.
62. Akcora, Pinar, et al. "Segmental dynamics in PMMA-grafted nanoparticle composites." Macromolecules 43.19 (2010): 8275-8281.
63. Hattemer, Gregory D., and Gaurav Arya. "Viscoelastic properties of polymer-grafted nanoparticle composites from molecular dynamics simulations." Macromolecules 48.4 (2015): 1240-1255.
64. Srivastava, Samanvaya, et al. "Self-suspended polymer grafted nanoparticles." Current Opinion in Chemical Engineering 16 (2017): 92-101.
65. Sen, Suchira, Sanat K. Kumar, and Pawel Keblinski. "Viscoelastic properties of polymer melts from equilibrium molecular dynamics simulations." Macromolecules 38.3 (2005): 650-653.
66. Kubo, Ryogo. "Statistical-mechanical theory of irreversible processes. I. General theory and simple applications to magnetic and conduction problems." Journal of the Physical Society of Japan 12.6 (1957): 570-586.
67. Kim, Daniel, et al. "Polymer nanocomposites: polymer and particle dynamics." Soft Matter 8.42 (2012): 10813-10818.
68. Pryamitsyn, Victor, and Venkat Ganesan. "Origins of Linear Viscoelastic Behavior of Polymer– Nanoparticle Composites." Macromolecules 39.2 (2006): 844-856.

69. Srivastava, Samanvaya, et al. "Hyperdiffusive dynamics in newtonian nanoparticle fluids." ACS Macro Letters 4.10 (2015): 1149-1153.

70. Kremer, Kurt, and Gary S. Grest. "Dynamics of entangled linear polymer melts: A molecular-dynamics simulation." The Journal of Chemical Physics 92.8 (1990): 5057-5086.

71. Martin, Tyler B., and Arthi Jayaraman. "Tuning the wetting–dewetting and dispersion–aggregation transitions in polymer nanocomposites using composition of graft and matrix polymers." Materials Research Express 3.3 (2016): 034001.

72. Srivastava, Samanvaya, Lynden A. Archer, and Suresh Narayanan. "Structure and transport anomalies in soft colloids." Physical review letters 110.14 (2013): 148302.